Blocking oligomerization is the most viable strategy to inhibit STING

Rebecca Chan[1,2,3,7], Xujun Cao[2,3,4,7], Sabrina L. Ergun[2,5], Evert Njomen[6], Stephen R. Lynch[4], Benjamin F. Cravatt[6], Lingyin Li[2,3,5,*]

[1]Department of Chemical and Systems Biology, Stanford University, Stanford, CA 94305, USA
[2]Sarafan ChEM-H Institute, Stanford University, Stanford, CA 94305, USA
[3]Arc Institute, Palo Alto, CA 94304, USA
[4]Department of Chemistry, Stanford University, Stanford, CA 94305, USA
[5]Department of Biochemistry, Stanford University, Stanford, CA 94305, USA
[6]Department of Chemistry, Scripps Research Institute, La Jolla, CA 92037, USA
[7]These authors contributed equally
*Correspondence: lingyinl@stanford.edu, lingyin@arcinstitute.org

Abstract

Autoimmune disorders are frequently exacerbated by aberrant STING signaling. While STING inhibitors are highly sought after, no viable therapeutic strategies have been reported. When stimulated, STING undergoes a multi-step mechanism to activate downstream interferon-stimulated genes (ISGs), including palmitoylation, translocation from the ER to the Golgi, and oligomerization, but it remains unclear which step(s) are strictly required and therefore should be targeted by potential STING inhibitors. Here, we comprehensively established the order and determined the necessity of each STING activation step. We find that ER-to-Golgi translocation is dispensable for downstream ISG activation, and a previously studied palmitoylation site, C91, is not required for activation in all contexts. Cysteine reactivity mapping and metabolic labeling identified a new palmitoylation site, C64, that is basally palmitoylated and required for STING activation, but is not druggable due to poor solvent accessibility. We confirm that the oligomerization step of STING activation is strictly required, and therefore developed a short peptide mimicking its natural autoinhibitory domain that effectively inhibits STING activation: a proof of concept for the first viable strategy for developing STING inhibitors.

Introduction

The innate immune system must be tightly regulated to avoid autoimmunity while responding appropriately to real threats. The STING pathway is a quintessential example where this delicate balance is maintained by many layers of regulatory mechanisms (Ablasser and Hur, 2020). The STING pathway is activated when double-stranded DNA (dsDNA) or DNA:RNA hybrids are detected in the cytosol by cyclic-GMP-AMP synthase (cGAS), which produces the second messenger 2',3'-cyclic-GMP-AMP (cGAMP) in response (Gao et al., 2013; Li et al., 2013; Mankan et al., 2014; Sun et al., 2013). cGAMP directly binds to STING, a transmembrane receptor that resides on the cytosolic face of the endoplasmic reticulum (ER) (Ablasser et al., 2013). Activated STING serves as a scaffold to bring the kinase TBK1 to the transcription factor IRF3, leading to phosphorylation, dimerization, and nuclear translocation of IRF3, which then activates the expression and secretion of type I interferons (Zhang et al., 2019; Zhao et al., 2019). These interferons have broad anti-viral effects and potently activate downstream immune cascades including recruitment of the adaptive immune system (Chen et al., 2011; Deng et al., 2014; Wang et al., 2019).

The STING pathway responds to cytosolic dsDNA and DNA:RNA hybrids, which are both PAMPs—originating from sources like viral infections, and DAMPs—arising from endogenous cellular events like mitochondrial damage or DNA replication errors (Li and Chen, 2018; Maekawa et al., 2019; Sliter et al., 2018). By virtue of their inherent abundance in the normal cell, these signatures are quite non-specific but have the potential to potently activate STING. Therefore, many DNA repair mechanisms (e.g. p53, BRCA, PARPs, RNase H) act to prevent DNA leakage into the cytosol and thereby disfavor autoimmune STING activation (Ablasser and Hur, 2020). Cytosolic dsDNA is also basally produced in our cells by reverse transcription of cytosolic RNAs, but its level is tightly constrained by cytosolic DNase Trex-1 and dNTP degrader SAMHD1 (Demaria, 2018; Maelfait et al., 2016).

When these regulatory mechanisms fail in the absence of real threats or when acute damages overwhelm the system, STING activation has harmful consequences. Aberrant STING activation has been implicated in hyperinflammatory responses in autoimmune diseases like systemic lupus erythematosus, multiple sclerosis, and Aicardi-Goutières syndrome (Ahn et al., 2012; Kumar, 2019; Lemos et al., 2014; Sharma et al., 2013), as well as in the context of myocardial infarction and pancreatitis (King et al., 2017; Zhao et al., 2018). Patients harboring activating mutations in STING develop STING-associated vasculopathy with onset during infancy (SAVI) (Jeremiah et al., 2014; Lin et al., 2020; Liu et al., 2014; Melki et al., 2017). As a result, major efforts have been made to develop STING inhibitors, but unfortunately none have advanced into clinical trials. Our current incomplete understanding of the molecular steps of STING activation has limited therapeutic progress on this important target.

Inactive STING exists as a stable dimer auto-inhibited by its C-terminal tail (CTT) (Ergun et al., 2019). When ligands such as cGAMP bind to its cytosolic ligand-binding domain (LBD), STING undergoes a conformational change that closes the LBD around cGAMP and rotates the cytosolic domain 180° relative to its transmembrane domain (Hopfner and

Hornung, 2020). Release of the CTT from its autoinhibitory binding site exposes STING's oligomerization interface, allowing it to form disulfide-stabilized oligomers via C148 (Ergun et al., 2019). The formation of STING oligomers then initiates an irreversible sequence that includes translocation from the ER to the Golgi and palmitoylation at the transmembrane cysteines C88 and C91, while the released CTT is arrayed on the STING oligomer to scaffold multivalent interactions between TBK1 and IRF3 for downstream signaling (Zhang et al., 2019; Zhao et al., 2016) (**Figure 1A**).

In principle, each of these steps—ligand binding, oligomerization, translocation, and palmitoylation could be pharmacologically targeted in pursuit of an inhibitor. Small molecule antagonists have been reported to target the LBD in direct competition with cGAMP (Hong et al., 2021; Li et al., 2018), a previously reported palmitoylation site C91 (Haag et al., 2018), and the disulfide site C148 (Humphries et al., 2023). The failure of most of these molecules to advance into the clinic since their discovery raises the question of whether these molecular steps are required for the activation of STING and are actually good targets for inhibitor development.

In this work, we examine the necessity and sufficiency of each step of STING translocation, palmitoylation, and oligomerization for downstream signaling. We report that neither trafficking to the Golgi nor palmitoylation at C91 is required for downstream STING signaling in all contexts. We mapped STING palmitoylation sites and determined that a previously undescribed residue, C64, is the crucial palmitoylation site, the modification of which allosterically allows C148 to form the crucial oligomer-stabilizing disulfide bond upon cGAMP binding. However, we show that C64 palmitoylation is poorly druggable due to a lack of accessibility to small molecule conjugation. Importantly, we show that STING oligomerization precedes all these events and is strictly necessary for STING activation. By systematically probing the mechanism of STING autoinhibition, we developed a short CTT-mimetic peptide that directly binds the STING oligomerization interface and completely blocks STING activation in response to cGAMP. Our proof-of-concept study demonstrates that STING oligomers have a druggable protein-protein interface and STING's autoinhibitory mechanism can be mimicked by small molecules, a viable strategy to developing potent and specific STING inhibitor drugs.

Results

STING oligomerization precedes all other steps in the activation sequence

Other studies have aimed to characterize the order and essentiality of the molecular events leading to STING activation, but different studies used different STING ligands (i.e. direct agonists like DMXAA or cGAMP, or dsDNA transfection to induce endogenous cGAMP production by cGAS) and different cell lines, making it impossible to merge individual findings into a cohesive picture of the entire process. For example, it has been previously shown that human STING expressed in mouse embryonic fibroblasts (MEFs) traffics to the Golgi 20–30 minutes post stimulation with DMXAA, a mouse-specific STING agonist (Mukai et al., 2016). While STING has been shown to form ER-associated bio-condensates upon dsDNA or cGAMP stimulation (Yu et al., 2021), others have shown that STING only forms higher order oligomers upon interaction with sGAGs in the Golgi lumen (Fang et al., 2021). STING was previously shown to be palmitoylated upon arrival at the Golgi, where its native palmitoylation enzymes are thought to reside (Mukai et al., 2016), but it remains unclear whether this happens before or after oligomerization, and exactly what role it plays in STING activation. Here, we systematically addressed each of these key mechanistic steps in HeLa Kyoto cells, a human cell line with an intact STING pathway.

In order to determine the sequence of molecular and cellular events during STING activation, we first performed a blue-native PAGE (BN-PAGE) assay in Hela Kyoto cells across a two-hour time course to quantify STING oligomerization. We found that oligomerization occurs rapidly, becoming saturated within 10 minutes of cGAMP addition and persisting across the entire time course (**Figure 1B**). In agreement with previous literature, we confirmed by fluorescence confocal microscopy that STING is primarily ER-localized in the absence of cGAMP and only translocates to the Golgi after addition of cGAMP to the media (**Figure S1A**). The majority of STING has translocated to the Golgi around 30 minutes after cGAMP addition, suggesting that the rapid STING oligomerization we observed within 10 minutes occurs at the ER before trafficking (**Figure 1C**). We also considered the alternative hypothesis that STING may constantly traffic between the ER and the Golgi, forming oligomers at the Golgi before cycling back to the ER on a much shorter time scale. To address this possibility, we isolated vesicles from cells using serial centrifugation (**Figure S1B**). We gently lysed these enriched vesicles and used BN-PAGE to measure the oligomerization state of STING when packaged in vesicles. We found that all vesicle-bound STING is entirely in the oligomer form, indicating that STING does not traffic as a monomer (**Figure S1C**). Finally, we monitored STING palmitoylation over the same timecourse using the established alkyne-labeled palmitate substrate followed by visualization using an azide-labeled fluorescent dye (Gao and Hannoush, 2018). We observed a surprising amount of basal palmitoylation before cGAMP stimulation (at $t = 0$), which increased over time concurrently with trafficking to twice the basal level (**Figure 1D**). This raises the intriguing possibility of multiple palmitoylation sites that could each be either basally modified or only modified in response to cGAMP stimulation. Taken together, we can infer from our timecourse analyses that STING oligomerization is cGAMP-dependent but occurs before trafficking to the Golgi, and that STING palmitoylation happens both basally at the ER and in a cGAMP-inducible fashion upon trafficking to the Golgi.

STING trafficking is not necessary or sufficient for STING activation

Since we observed that STING is already oligomerized and basally palmitoylated at the ER, this raised the question of whether STING trafficking from the ER to Golgi is necessary for its activation. Published studies of STING trafficking typically use blunt force methods such as Brefeldin A or nocodazole to perturb intracellular transport, but interpretation of the results is challenging since these treatments collapse the Golgi and therefore have broad effects on cellular function. Instead, we chose to use a selective tool called Retention Using Selective Hooks (RUSH), which can be used to specially control whether STING is localized at the ER or at the Golgi without changing other aspects of cell biology (**Figure 2A**) (Boncompain et al., 2012). We first validated that RUSH-STING could be retained at the ER by measuring the amount of STING-Golgi colocalization with and without biotin, the trigger for release of the RUSH moiety from the ER. Although ~20% of STING seemed to be present at the Golgi without biotin, there was significantly more STING-Golgi colocalization (>70%) with the addition of biotin as expected, suggesting that release of STING to the Golgi has occurred (**Figures 2B, C**). Having validated this system, we then measured the level of STING activation by quantifying pIRF3 levels and IFN-β secretion in cGAMP-stimulated cells with or without biotin. We observed comparable amounts of STING activation upon treating RUSH-STING-expressing cells with cGAMP alone or both cGAMP and biotin, but not with biotin alone (**Figures 2D, S2**). Given that we achieved the same amount of STING activation despite more than three-fold difference in Golgi localization, we infer that STING can fully signal without trafficking to the Golgi. Together, we conclude that trafficking of STING is not necessary or sufficient for its activation. While endogenous STING might still only activate TBK1 and IRF3 at the Golgi, our fusion system strongly suggests that inhibiting STING trafficking by manipulating potential trafficking factors (Zhang et al., 2020) or retention factors (Srikanth et al., 2019) is not a viable therapeutic strategy because the STING-IFN-β pathway is fully active even when forcibly retained at the ER.

Palmitoylation at C64 alone but not C91 is necessary for activation

Cysteines 88 and 91 (C88 and C91) are thought to be the predominant sites of STING palmitoylation (Haag et al., 2018; Mukai et al., 2016). We created mutations at either C88 (STING-C88S), C91 (STING-C91S) or both cysteines (STING-C88/91S) to understand their contributions to STING activation. For this and all subsequent studies, cysteine was mutated to serine, maintaining the polar side chain to minimize impact on protein folding. Additionally, C88 and C91, along with other transmembrane cysteines (C12, C29, C64, **Figure 3A**), are not known to form disulfide bonds. Therefore, we expect the serine mutants to primarily disrupt palmitoylation. To our surprise, we observed significant amount of palmitoylation in both of these mutants (**Figure 3B, S3A**), indicating that STING must also be palmitoylated at other previously undescribed site(s). We also observed comparable levels of pIRF3 and IFN-β in both of these cysteine mutants compared to wild-type STING, indicating that C88 and C91 are not necessary for STING palmitoylation or activation (**Figures 3D, S3C**).

To identify other palmitoylation sites and investigate their role in STING signaling, we mutated all five cysteines (C12, C29, C64, C88 and C91) within STING's transmembrane domain to serine individually. We observed that only the C64S mutation abrogated STING

activation. We then asked whether C64 or C91 is sufficient for STING palmitoylation and activation by mutating all five cysteines (5C5S) and then adding back either residue individually. In the cysteine-less mutant 5C5S, we observed little to no palmitoylation along with a complete absence of STING activity, supporting the notion in the field that palmitoylation is indeed necessary for STING activation (**Figures 3C, S3B**). Adding back C91 (5C5S+91) yielded virtually no basal palmitoylation and only a marginal increase upon cGAMP addition, but we could not detect pIRF3 and IFN-β indicating that STING remains inactive for downstream signaling (**Figures 3E, S3D**). In contrast, adding back C64 (5C5S+64) yielded basal palmitoylation (**Figure 3C**), which did not increase upon cGAMP stimulation. This mutant restored STING activity in response to cGAMP stimulation to a similar level as WT STING (**Figures 3E, S3D**), implying that basal palmitoylation at C64 is necessary for STING activation, but cGAMP stimulation is still required. In contrast, the single cysteine mutant C64S has observable levels of basal palmitoylation which does not increase significantly upon stimulation with cGAMP and this mutant has impaired activity (**Figures 3D, E**), supporting a model where, while palmitoylation could also occur in a compensatory fashion in the absence of C64 (i.e. C88 or C91), such palmitoylation is inconsequential and C64 palmitoylation is necessary for STING activation.

C64 palmitoylation prevents unproductive STING aggregation

We then asked why C64's basal palmitoylation is crucial for STING activation. We and others previously showed that oligomerization is necessary for all downstream activation processes, and oligomerization-defective mutants are unable to activate TBK1 (Ergun et al., 2019; Shang et al., 2019; Zhang et al., 2019). Since oligomerization is required for STING signaling, we hypothesized that the C64S mutant has oligomerization defects. Indeed, our BN-PAGE assay showed that C64S and 5C5S, but not C88/91S form much higher molecular weight aggregates than the active oligomers seen in WT STING or 5C5S+64 (**Figures 3F, S3H**). Previous structural work from our group and others suggested that ordered STING oligomers present an array of its C-terminal tails (CTTs) that scaffold TBK1 and IRF3 interaction (Zhao et al., 2019, 2016). We show that, while C64S STING aggregates can still bind overexpressed TBK1 in a co-immunoprecipitation assay (**Figure 3G**) and be phosphorylated by both endogenous and overexpressed TBK1, they cannot enable IRF3 phosphorylation by TBK1 (**Figure 3H**), suggesting that this C64S mutant presents a defective CTT scaffold. Together, our results suggest that C64 basal palmitoylation is important for preventing cGAMP-independent aggregates, possibly by maintaining the correct transmembrane conformation.

Since C64 is crucial for STING activation, we asked whether it can be inhibited by cysteine-reactive compounds. We analyzed our previous proteomics data identifying reactive cysteines. C64 does not possess any reactivity even to the non-specific and highly reactive iodoacetamide desthiobiotin (IA-DTB) probe, suggesting either it is buried and only accessible to enzyme-mediated palmitoylation, or that its basal palmitoylation prevents it from being chemically modified. Therefore, this linchpin palmitoylation site, while important for STING signaling, appears to be a challenging residue to target therapeutically due to its inaccessibility. We therefore continued to evaluate other avenues to inhibit STING signaling.

C91 allosterically controls C148 reactivity in a cell type-dependent manner

C91 reactive compounds have served as important tools in the human malignant monocytic THP-1 cell line as well as in mouse models of autoimmune diseases, aging and interferonopathies (Domizio et al., 2022; Gulen et al., 2023; Haag et al., 2018). We were however puzzled by the fact that C91 does not seem crucial in our study system. Indeed, H-151, the most studied C91 reactive compound, did not inhibit STING signaling in our 293T system either (**Figure S4A**). Given the conflicting results in these different contexts, we tested H-151's efficacy at inhibiting STING activation across a panel of cell types. Indeed, H-151 is most effective in malignant monocytic cell lines where it has been used previously, but not in primary human PBMCs and some other cell lines (**Figures S4A, B**). To investigate this cell type specificity further, we probed how C91-reactivity leads to STING inhibition in THP-1. In our whole-proteomic reactive cysteine profiling dataset, we identified compounds **58** and **60** that react to C91, indicated by their lowered reactivity to non-specific acetylation by our IA-DTB probe, while their stereoisomers **57** and **59** do not (**Figures 4A, B**). Using **58** and **60** as tool compounds and their inactive stereoisomers as controls, we studied STING inhibition in U937 cells, another cancerous cell line along the same developmental lineage as THP-1. We observed that compounds **58** and **60**, but not **57** and **59**, could indeed inhibit STING signaling similarly to H-151 (**Figures 4C, S4A**). We then asked whether the reactivity of any other cysteine(s) on STING may be allosterically controlled by these modifications on C91. Strikingly, C148, the known disulfide-forming residue (Ergun et al., 2019), exerted a large increase in reactivity upon C91 engagement by compounds **58** and **60** both with and without cGAMP treatment (**Figure 4D**). An increase in C148 reactivity suggests a lack of disulfide bonds at this site, pointing to a model where STING C91-reactive compounds block STING signaling by allosterically inhibiting disulfide stabilization of STING oligomers at C148. Although we previously proposed that this indicated STING oligomers stabilized by disulfide formation between C148 of adjacent STING dimers, recently published cryo-EM structures of cGAMP-bound, full-length STING (Liu et al., 2023; Lu et al., 2022) suggested that, compared to apo STING, (Shang et al., 2019), the positions of the two C148 residues did not change significantly, and remained too distant to engage in disulfide formation with neighboring units. Therefore, C148 mediates an intra-dimer disulfide bond.

We then tested whether this mechanism also occurs in our 293T model cell line system. We tested direct conjugation of H-151 to C91 by incubating cells expressing STING variants with H-151 containing an alkyne handle (H151-AL) (Haag et al., 2018). Following enrichment and conjugation with an azide-containing fluorescent label, we saw that H151-AL could conjugate onto wild-type STING but not the 5C5S mutant (**Figure 4E**). Interestingly, H151-AL reacted with 5C5S STING with both C64 and C91 added back, but not when only C91 was added back, suggesting C64 is required for C91 reactivity, possibly by the same mechanism of ensuring the correct transmembrane conformation. Since H-151 can properly conjugate onto C91 in 293T cells, we asked whether it also blocks disulfide formation through C148 like in THP-1 cells. In agreement with its lack of efficacy in inhibiting STING activity, H-151 did not inhibit cGAMP-induced disulfide formation in non-reducing SDS gel assays, but did increase basal disulfide interactions

similar to the C91S mutant (**Figure 4F**). Since any modification of C91, genetic or chemical, appear to exhibit highly cell type-dependent effects, we conclude that palmitoylation is an indirect and context-dependent regulator of STING activation that would not be a promising drug target.

Since C91 allosterically controls C148 reactivity, we asked whether C64 palmitoylation also controls C148 reactivity. Indeed, C64S and 5C5S, which are inactive STING mutants, showed substantial amount of disulfide without cGAMP induction while the active 5C5S with C64 added back did not (**Figure 4G**). We do not know, however, whether C64S allosterically induced premature C148 disulfide bonding first which in turn induces transmembrane domain aggregation, or if it is the other way around.

Defining residues important for STING autoinhibition

We previously reported that STING's unstructured C-terminal tail (CTT, aa 340–379) plays an autoinhibitory role in unliganded, inactive STING. Upon cGAMP binding, the autoinhibition is relieved, allowing STING to polymerize and initiate downstream signaling events. We also showed that overexpression of the CTT *in trans* can inhibit STING oligomerization and subsequent interferon signaling even upon cGAMP stimulation (Ergun et al., 2019). Furthermore, mutations on the STING surface that prevent CTT engagement and disrupt this autoinhibition mechanism (e.g. STING R284S) are associated with the autoimmune disease SAVI, emphasizing the importance of CTT autoinhibition to constrain aberrant STING activation (Konno et al., 2018). We, therefore, turned our attention to probing and harnessing the mechanism of STING autoinhibition to develop potential strategies to inhibit STING oligomerization.

Despite numerous efforts from us and others, the structure of STING CTT and how it binds STING remain elusive, suggesting the entire CTT is highly flexible and its binding to STING is dynamic. Taking our cue from SAVI-associated mutations, we reasoned that STING residues at the CTT binding site can be identified by mutagenesis screening: mutants that lose affinity for CTT would become constitutively active in the absence of cGAMP stimulus. We therefore transiently overexpressed a panel of single alanine mutations of STING in 293T-Dual cells and measured levels of luciferase activity indicative of STING-induced interferon activation in the absence of cGAMP. We indeed identified three hyperactive mutants, with two of them (Q315A and D320A) occurring near R284 and another SAVI-associated residue, R281 (Lin et al., 2020; Wang et al., 2021) (**Figure 5A**). The third residue, E366, was found on the opposite side of the STING body and has been reported as important for phase separation-mediated restraint of STING signaling (Yu et al., 2021). This mutagenesis work therefore localized a possible CTT binding site on STING.

We then turned our attention to the CTT itself with the aim of identifying the minimal unit that retains inhibitory activity, since this moiety could inform the design and screening of potential inhibitors for this site. We truncated the 39-amino acid CTT into three segments (CTT1, aa340–353; CTT2, aa 354–366; CTT3, aa 367–379) (**Figure 5B**) and expressed each HA-tagged segment as bait to co-immunoprecipitate STING (**Figure S5A**). We observed that CTT1 and CTT3 were able to bind to STING, but CTT2 was not. We then

expressed either CTT1 or CTT3 in 293T-Dual cells also transiently expressing wild-type STING, and tested the effects of CTT segment expression on interferon activity stimulated by cGAMP. Only CTT3 over-expression was able to inhibit cGAMP-induced STING activity (**Figure S5C**). Using confocal microscopy, we also showed that CTT3, but not CTT1, was able to inhibit the formation of STING puncta (**Figure S5B**), indicating that it is the relevant segment in the inhibition of STING oligomerization. By further dividing CTT3 into two smaller segments, we observed that a seven-residue unit (MEKPLPL, hereon referred to as CTT7, aa368–374) was sufficient to significantly inhibit cGAMP-induced interferon signaling (**Figure 5C**).

CTT7 contains half of the sequence (PLPLRTD) known to bind to TBK1, STING's downstream interacting partner (**Figure 5B**) (Zhao et al., 2019), raising the possibility that it may inhibit TBK1 instead of directly inhibiting STING itself. However, we do not believe that this is the case, because overexpression of CTT7 abolished the formation of STING puncta following cGAMP treatment (**Figure 5D**). To further confirm that CTT7 is not acting at the level of TBK1, we also tested a different seven-residue peptide containing the latter half of the TBK1-binding moiety (PLRTDFS, which we refer to as nCTT7) and showed that it did not inhibit STING signaling nor oligomerization (**Figures 5C, D**).

CTT7 inhibits STING oligomerization by directly inhibiting the STING–STING interaction

To directly test binding of CTT7 to STING, we synthesized an ^{15}N-labelled CTT7 peptide and examined its behavior with ^{15}N–^{1}H HSQC NMR spectroscopy (**Figure 6A**). CTT7 demonstrated high flexibility and we could reliably detect signals from only three of the four NMR-active amidic ^{15}N. Although we could not confidently assign the peaks to specific nitrogen atoms, we observed that addition of one molar equivalent of purified STING cytosolic domain (STING residues 138-366) caused a clear upfield shift of the proton signal for the ^{15}N–^{1}H correlation peaks suggesting changes to local environment of the ^{15}N-labelled peptide due to binding interactions. Furthermore, addition of the NMR-invisible ^{14}N-CTT to a similarly prepared sample abolished this shift, suggesting direct competition between the peptide fragments for a shared binding site.

In our reported model of STING autoinhibition (Ergun et al., 2019), we anticipated that the large conformational change in STING caused by cGAMP binding was responsible for the dissociation of the autoinhibitory CTT. We therefore expected that binding of the CTT and cGAMP at distinct sites on the STING body are mutually allosteric. However, to our surprise, in our NMR studies, addition of cGAMP to ^{15}N-CTT7 incubated with STING cytosolic domain did not restore the free ^{15}N-CTT7 spectrum. Furthermore, we performed the reciprocal experiment and were likewise unable to compete with the binding of ^{32}P-labelled cGAMP to STING using large concentrations of any fragment of CTT (**Figure 6B**). While these results do not exclude a possible role of the transmembrane domain of STING in mediating either CTT binding or cGAMP–CTT allostery, they nevertheless indicate that cGAMP and CTT can bind STING simultaneously.

Since cGAMP binding does not preclude CTT binding of STING, we next asked how the CTT is released to activate STING in the cellular context. Through co-immunoprecipitation

experiments using CTT7–FLAG as bait, we first orthogonally verified that STING indeed binds to CTT7, and that the addition of cGAMP reduces this affinity (**Figure 6C**), in agreement with our prior work (Ergun et al., 2019). Crucially, when we performed the same experiment with an oligomerization-defective STING mutant (Q273A/A277Q) (Shang et al., 2019), cGAMP was no longer able to reduce STING's affinity to CTT7. These data indicate that the intra-oligomer STING–STING interaction, but not binding of cGAMP, is principally responsible for abolishing STING–CTT interactions to activate STING signaling.

Residue–activity relationship studies of CTT in inhibiting STING

Referring to a crystal structure of the apo STING cytosolic domain (PDB: 4F5W), we identified a candidate binding site for the CTT7 peptide close to the key STING residues R284, R281, Q315, and D320 that we highlighted in our hyperactivation screen above (**Figures 5A, 7A**). We computationally docked CTT7 into this putative binding pocket and hypothesized that CTT could form a salt bridge at this site between STING R284 and CTT7 glutamate E369 (numbered by its original position in the full-length STING sequence). We validated this experimentally with co-immunoprecipitation experiments (**Figure 7B**): CTT7 had diminished affinity with a charge-switched R284E mutant of STING, and, reciprocally, the CTT7-E369R peptide had diminished affinity with wild-type STING. Importantly, CTT7-E369R could co-immunoprecipitate STING R284E in an enhanced manner, constituting a pair where the potential salt bridge was restored by compensatory mutation. In agreement with these co-immunoprecipitation results, E369A-CTT7 (MAKPLPL) (**Figure S6**) was no longer able to inhibit STING signaling in our interferon reporter assay. This observation lends strong support to the importance of a salt bridge in maintaining STING–CTT interaction at this location on the STING body.

We also noted that, among the top docking poses, the N-terminal methionine of CTT7 is not predicted to sufficiently occupy a hydrophobic pocket-like site proximal to the critical R–E salt bridge (**Figure 7A**). We thus lengthened the CTT with the addition of a hydrophobic phenylalanine residue at position 2 in an attempt to stabilize binding on this N-terminal side of the salt bridge, and found that the resultant 8-mer (MFEKPLPL) showed improved inhibitory properties compared to the original CTT (**Figure 7D**). Taken together, we have identified the CTT7 binding site on STING and specific molecular interactions that govern its binding.

Discussion

In detailing the fundamental mechanisms and signaling events that are important for STING activation and inhibition, we uncovered several key principles that challenge current assumptions in the field and hold major implications for STING inhibitor development. By profiling the temporal order and dependencies between the mechanistic steps of STING activation, we unify past and present findings to conclude that STING oligomerization is the key step to target for effective future STING inhibitors.

Learning from STING's natural autoinhibitory mechanism, we find that the CTT binds the STING body at the same site where a neighboring STING dimer would normally bind to form active STING oligomers. Though this interaction is weak in apo STING, it has low

entropic penalty, being an intramolecular interaction between the LBD and the CTT that is anchored to it. Upon cGAMP binding, the angle of the STING dimer, which is usually flexible, becomes fixed (Ergun et al., 2019; Lu et al., 2022; Shang et al., 2019), and the two linkers between the cytosolic domain and transmembrane region untwist (Liu et al., 2023; Lu et al., 2022) and are covalently linked by the intradimer disulfide bond formed between two C148 residues. The loss of these two degrees of freedom reduces the entropic penalty of STING–STING interactions and promotes oligomer formation, simultaneously representing a new competing force that displaces the autoinhibiting CTT (**Figure 8**). The dynamic competition between the neighboring STING dimer and the autoinhibitory CTT predicts that higher STING dimer concentrations would favor their oligomerization. In support of this model, overexpression of STING alone in cell lines is often sufficient to induce activation. Furthermore, in the lysosomal storage disease Niemann Pick disease type C, STING is not degraded efficiently and retained at the Golgi, resulting in tonic STING signaling in the absence of external PAMPs/DAMPs that drives inflammatory phenotypes (Chu et al., 2021). Thus, regardless of location, oligomerization appears to be the most important step in STING activation.

Other studies have posited that palmitoylation serves to promote clustering of STING and partitioning into lipid rafts to promote TBK1 and IRF3 association (Fang et al., 2021; Mukai et al., 2016). We have shown that this model must be revised: our 5C5S mutant, which lacks all transmembrane cysteines and cannot be palmitoylated at all, as well as STING mutants lacking what were thought to be key palmitoylation residues C88 and C91, can all still form higher order oligomers. Our data, however, suggest that the major role of STING palmitoylation at C64 is to prevent an unproductive C148 disulfide-linked aggregate from forming in the absence of stimuli, ensuring a transmembrane domain conformation that can be responsive to cGAMP. Our conclusion that C91 is not strictly necessary for STING signaling contradicts prior studies (Haag et al., 2018; Mukai et al., 2016), indicating that the role of C91 in STING signaling is still contentious. However, our results that H-151 and other C91-reactive compounds are only effective in very limited cell types is consistent with the observation in the field that H-151 is ineffective in primary human T cells (An et al., 2023).

From a therapeutic standpoint, these transmembrane and linker region cysteines are nevertheless challenging targets. C148 is a key target for inhibiting oligomerization, but resides within a flexible linker region of STING that would be a very poorly druggable site. The recently published C148-reactive STING inhibitor BB-Cl-amidine, as a tool compound, highlighted the importance of C148 in forming STING oligomers (Humphries et al., 2023). However, this inhibitor remains non-specific and is indeed better known as a pan-protein arginine deiminase inhibitor. C91 targeting suffers from two caveats: (1) like C148, it lacks a distinct druggable pocket with stereospecificity since the diastereomeric compounds **58** and **60** can both conjugate onto the residue; (2) its efficacy in inhibiting C148 disulfide bonding is cell type-dependent. We have shown that C64 is important for preventing the formation of dead STING aggregates. However, since C64 is not chemically reactive, at least in THP-1 cells, we do not believe it is a good site for inhibitor development.

We showed that intracellular trafficking of STING is not required for its activation, nor does it play a role in oligomerization or palmitoylation, which can both occur at the ER prior to STING's translocation to the Golgi. Though there are Golgi-resident palmitoylation enzymes known to act on STING, there are also ER-resident palmitoylation enzymes that we hypothesize could facilitate this basal ER-localized palmitoylation. We speculate that trafficking may purely serve to promote STING degradation or turnover. Importantly, our model predicts that inhibiting STING trafficking by manipulating potential trafficking factors or retention factors (Srikanth et al., 2019; Zhang et al., 2020) would not an effective therapeutic strategy because STING is active even when artificially retained at the ER.

Considering the limitations of targeting palmitoylation and trafficking, then, blocking oligomerization appears to be the most promising strategy in the inhibition of STING. Moreover, our model of autoinhibition of STING by CTT presents the CTT and its binding site on the STING body as a lead candidate to recapitulate this endogenous mechanism. Building on our previous finding that overexpression of CTT can reduce STING activation by cGAMP (REF), we now localize this inhibitory effect to seven residues located near the end of the CTT. Furthermore, we provide evidence that this minimal CTT unit binds to a defined site on the STING LBD that is available regardless of cGAMP binding – an important consideration for therapeutic development – and performed proof-of-concept mutagenesis studies suggesting that this site exerts a structure-activity relationship. By defining this previously unexplored CTT binding site, we have now provided the most promising druggable site on STING.

Finally, while our identification of oligomerization as the key therapeutically relevant step to block STING activation has strong implications for future STING therapeutics, we also believe that these findings will have broader conceptual implications for understanding and targeting the innate immune system in other contexts. Oligomerization is a thresholding mechanism common to the activation of many innate immune pathways, including RIG-I, NLRP3, and even primordial bacterial immune systems (Hafner-Bratkovič et al., 2018; Morehouse et al., 2020; Rehwinkel and Gack, 2020), its main role being thought to be preventing stochastic signals from aberrantly triggering immunity. From this viewpoint, our therapeutic approach centered on targeting oligomerization may have applications amongst vast branches and hierarchies of innate immunity.

Acknowledgements
We thank April Pawluk and the Arc Institute Scientific Publications Team for constructive feedback on the manuscript. We thank the lab of Peter Kim for providing access to peptide synthesis equipment. We thank Martha Cyert for her helpful discussion and suggestion on palmitoylation research, and all other Li Lab members for their constructive comments and discussion through the course of this study. R.C. thanks the Stanford Graduate Student Fellowship. L.L acknowledges her Stanford startup fund and Arc Institute funding.

Author Contributions
R.C. and X.C. conceived the project, performed the experiments, analyzed results, coordinated the project, and wrote the manuscript with input from all authors. S.L.E conceived the project, performed the experiments and analyzed results. E.N. performed

the chemoproteomic experiments and analyzed results. S.R.L. performed the NMR experiment and analyzed results. B.F.C. supervised E.N., provided scientific expertise, coordinated the project, and approved the final manuscript. L.L. conceived the project, coordinated the project, wrote the manuscript, and provided the project funding.

Declarations of Interests

The authors do not declare competing financial conflicts of interest.

References

1. Ablasser, A., Goldeck, M., Cavlar, T., Deimling, T., Witte, G., Röhl, I., Hopfner, K.-P., Ludwig, J., Hornung, V., 2013. cGAS produces a 2′-5′-linked cyclic dinucleotide second messenger that activates STING. Nature 498, 380–384. https://doi.org/10.1038/nature12306
2. Ablasser, A., Hur, S., 2020. Regulation of cGAS- and RLR-mediated immunity to nucleic acids. Nat Immunol 21, 17–29. https://doi.org/10.1038/s41590-019-0556-1
3. Ahn, J., Gutman, D., Saijo, S., Barber, G.N., 2012. STING manifests self DNA-dependent inflammatory disease. Proceedings of the National Academy of Sciences of the United States of America 109, 19386–19391. https://doi.org/10.1073/pnas.1215006109
4. An, J., Zhang, C.-P., Qiu, H.-Y., Zhang, H.-X., Chen, Q.-B., Zhang, Y.-M., Lei, X.-L., Zhang, C.-X., Yin, H., Zhang, Y., 2023. Enhancement of the viability of T cells electroporated with DNA via osmotic dampening of the DNA-sensing cGAS–STING pathway. Nat. Biomed. Eng 1–16. https://doi.org/10.1038/s41551-023-01073-7
5. Boncompain, G., Divoux, S., Gareil, N., de Forges, H., Lescure, A., Latreche, L., Mercanti, V., Jollivet, F., Raposo, G., Perez, F., 2012. Synchronization of secretory protein traffic in populations of cells. Nat Methods 9, 493–498. https://doi.org/10.1038/nmeth.1928
6. Chen, H., Sun, H., You, F., Sun, W., Zhou, X., Chen, L., Yang, J., Wang, Y., Tang, H., Guan, Y., Xia, W., Gu, J., Ishikawa, H., Gutman, D., Barber, G., Qin, Z., Jiang, Z., 2011. Activation of STAT6 by STING Is Critical for Antiviral Innate Immunity. Cell 147, 436–446. https://doi.org/10.1016/j.cell.2011.09.022
7. Chu, T.-T., Tu, X., Yang, K., Wu, J., Repa, J.J., Yan, N., 2021. Tonic prime-boost of STING signalling mediates Niemann–Pick disease type C. Nature 596, 570–575. https://doi.org/10.1038/s41586-021-03762-2
8. Cravatt, B., Njomen, E., Hayward, R., DeMeester, K., Ogasawara, D., Dix, M., Nguyen, T., Ashby, P., Simon, G., Schreiber, S., Melillo, B., 2023. Comprehensive Mapping of Electrophilic Small Molecule-Protein Interactions in Human Cells. https://doi.org/10.26434/chemrxiv-2023-s446n
9. Demaria, S., 2018. TREX1 as a gate-keeper of cGAS/STING-mediated activation of interferon type I in cancer cells treated with DNA-damaging agents. Annals of Oncology 29, iii1. https://doi.org/10.1093/annonc/mdy046
10. Deng, L., Liang, H., Xu, M., Yang, X., Burnette, B., Arina, A., Li, X.-D., Mauceri, H., Beckett, M., Darga, T., Huang, X., Gajewski, T.F., Chen, Z.J., Fu, Y.-X., Weichselbaum, R.R., 2014. STING-Dependent Cytosolic DNA Sensing Promotes Radiation-Induced Type I Interferon-Dependent Antitumor Immunity in Immunogenic Tumors. Immunity 41, 843–852. https://doi.org/10.1016/j.immuni.2014.10.019

11. Domizio, J.D., Gulen, M.F., Saidoune, F., Thacker, V.V., Yatim, A., Sharma, K., Nass, T., Guenova, E., Schaller, M., Conrad, C., Goepfert, C., de Leval, L., Garnier, C. von, Berezowska, S., Dubois, A., Gilliet, M., Ablasser, A., 2022. The cGAS–STING pathway drives type I IFN immunopathology in COVID-19. Nature 603, 145–151. https://doi.org/10.1038/s41586-022-04421-w
12. Ergun, S.L., Fernandez, D., Weiss, T.M., Li, L., 2019. STING Polymer Structure Reveals Mechanisms for Activation, Hyperactivation, and Inhibition. Cell 178, 290-301.e10. https://doi.org/10.1016/j.cell.2019.05.036
13. Fang, R., Jiang, Q., Guan, Y., Gao, P., Zhang, R., Zhao, Z., Jiang, Z., 2021. Golgi apparatus-synthesized sulfated glycosaminoglycans mediate polymerization and activation of the cGAMP sensor STING. Immunity 54, 962-975.e8. https://doi.org/10.1016/j.immuni.2021.03.011
14. Gao, P., Ascano, M., Wu, Y., Barchet, W., Gaffney, B.L., Zillinger, T., Serganov, A.A., Liu, Y., Jones, R.A., Hartmann, G., Tuschl, T., Patel, D.J., 2013. Cyclic [G(2′,5′)pA(3′,5′)p] Is the Metazoan Second Messenger Produced by DNA-Activated Cyclic GMP-AMP Synthase. Cell 153, 1094–1107. https://doi.org/10.1016/j.cell.2013.04.046
15. Gao, X., Hannoush, R.N., 2018. A Decade of Click Chemistry in Protein Palmitoylation: Impact on Discovery and New Biology. Cell Chemical Biology 25, 236–246. https://doi.org/10.1016/j.chembiol.2017.12.002
16. Gulen, M.F., Samson, N., Keller, A., Schwabenland, M., Liu, C., Glück, S., Thacker, V.V., Favre, L., Mangeat, B., Kroese, L.J., Krimpenfort, P., Prinz, M., Ablasser, A., 2023. cGAS–STING drives ageing-related inflammation and neurodegeneration. Nature 620, 374–380. https://doi.org/10.1038/s41586-023-06373-1
17. Haag, S.M., Gulen, M.F., Reymond, L., Gibelin, A., Abrami, L., Decout, A., Heymann, M., van der Goot, F.G., Turcatti, G., Behrendt, R., Ablasser, A., 2018. Targeting STING with covalent small-molecule inhibitors. Nature 559, 269–273. https://doi.org/10.1038/s41586-018-0287-8
18. Hafner-Bratkovič, I., Sušjan, P., Lainšček, D., Tapia-Abellán, A., Cerović, K., Kadunc, L., Angosto-Bazarra, D., Pelegrin, P., Jerala, R., 2018. NLRP3 lacking the leucine-rich repeat domain can be fully activated via the canonical inflammasome pathway. Nat Commun 9, 5182. https://doi.org/10.1038/s41467-018-07573-4
19. Hong, Z., Mei, J., Li, C., Bai, G., Maimaiti, M., Hu, H., Yu, W., Sun, L., Zhang, L., Cheng, D., Liao, Y., Li, S., You, Y., Sun, H., Huang, J., Liu, X., Lieberman, J., Wang, C., 2021. STING inhibitors target the cyclic dinucleotide binding pocket. Proceedings of the National Academy of Sciences 118, e2105465118. https://doi.org/10.1073/pnas.2105465118
20. Hopfner, K.-P., Hornung, V., 2020. Molecular mechanisms and cellular functions of cGAS–STING signalling. Nat Rev Mol Cell Biol 21, 501–521. https://doi.org/10.1038/s41580-020-0244-x
21. Humphries, F., Shmuel-Galia, L., Jiang, Z., Zhou, J.Y., Barasa, L., Mondal, S., Wilson, R., Sultana, N., Shaffer, S.A., Ng, S.-L., Pesiridis, G.S., Thompson, P.R., Fitzgerald, K.A., 2023. Targeting STING oligomerization with small-molecule inhibitors. Proceedings of the National Academy of Sciences 120, e2305420120. https://doi.org/10.1073/pnas.2305420120

22. Jeremiah, N., Neven, B., Gentili, M., Callebaut, I., Maschalidi, S., Stolzenberg, M.-C., Goudin, N., Frémond, M.-L., Nitschke, P., Molina, T.J., Blanche, S., Picard, C., Rice, G.I., Crow, Y.J., Manel, N., Fischer, A., Bader-Meunier, B., Rieux-Laucat, F., 2014. Inherited STING-activating mutation underlies a familial inflammatory syndrome with lupus-like manifestations. J Clin Invest 124, 5516–5520. https://doi.org/10.1172/JCI79100
23. King, K.R., Aguirre, A.D., Ye, Y.X., Sun, Y., Roh, J.D., Ng, R.P., Kohler, R.H., Arlauckas, S.P., Yoshiko, V., Savo, A., Sadreyev, R.I., Kelly, M., Fitzgibbons, T.P., Fitzgerald, K.A., Mitchison, T., Libby, P., Nahrendorf, M., Weissleder, R., 2017. IRF3 and type i interferons fuel a fatal response to myocardial infarction. Nature Medicine 23, 1481–1487. https://doi.org/10.1038/nm.4428
24. Konno, H., Chinn, I.K., Hong, D., Orange, J.S., Lupski, J.R., Mendoza, A., Pedroza, L.A., Barber, G.N., 2018. Pro-inflammation Associated with a Gain-of-Function Mutation (R284S) in the Innate Immune Sensor STING. Cell Reports 23, 1112–1123. https://doi.org/10.1016/j.celrep.2018.03.115
25. Kumar, V., 2019. A STING to inflammation and autoimmunity. Journal of Leukocyte Biology. https://doi.org/10.1002/JLB.4MIR1018-397RR
26. Lemos, H., Huang, L., Chandler, P.R., Mohamed, E., Souza, G.R., Li, L., Pacholczyk, G., Barber, G.N., Hayakawa, Y., Munn, D.H., Mellor, A.L., 2014. Activation of the STING Adaptor Attenuates Experimental Autoimmune Encephalitis. The Journal of Immunology 192, 5571–5578. https://doi.org/10.4049/jimmunol.1303258
27. Li, S., Hong, Z., Wang, Z., Li, F., Mei, J., Huang, L., Lou, X., Zhao, S., Song, L., Chen, W., Wang, Qiang, Liu, H., Cai, Y., Yu, H., Xu, H., Zeng, G., Wang, Quanyi, Zhu, J., Liu, X., Tan, N., Wang, C., 2018. The Cyclopeptide Astin C Specifically Inhibits the Innate Immune CDN Sensor STING. Cell Reports 25, 3405-3421.e7. https://doi.org/10.1016/j.celrep.2018.11.097
28. Li, T., Chen, Z.J., 2018. The cGAS–cGAMP–STING pathway connects DNA damage to inflammation, senescence, and cancer. J Exp Med 215, 1287–1299. https://doi.org/10.1084/jem.20180139
29. Li, X., Shu, C., Yi, G., Chaton, C.T., Shelton, C.L., Diao, J., Zuo, X., Kao, C.C., Herr, A.B., Li, P., 2013. Cyclic GMP-AMP Synthase Is Activated by Double-Stranded DNA-Induced Oligomerization. Immunity 39, 1019–1031. https://doi.org/10.1016/j.immuni.2013.10.019
30. Lin, B., Berard, R., Rasheed, A.A., Aladba, B., Kranzusch, P.J., Henderlight, M., Grom, A., Kahle, D., Torreggiani, S., Aue, A.G., Mitchell, J., Jesus, A.A. de, Schulert, G.S., Goldbach-Mansky, R., 2020. A novel STING1 variant causes a recessive form of STING-associated vasculopathy with onset in infancy (SAVI). Journal of Allergy and Clinical Immunology 146, 1204-1208.e6. https://doi.org/10.1016/j.jaci.2020.06.032
31. Liu, Sheng, Yang, B., Hou, Y., Cui, K., Yang, X., Li, Xiaoxiong, Chen, L., Liu, Shichao, Zhang, Z., Jia, Y., Xie, Y., Xue, Y., Li, Xiaomei, Yan, B., Wu, C., Deng, W., Qi, J., Lu, D., Gao, G.F., Wang, P., Shang, G., 2023. The mechanism of STING autoinhibition and activation. Molecular Cell 83, 1502-1518.e10. https://doi.org/10.1016/j.molcel.2023.03.029
32. Liu, Y., Jesus, A.A., Marrero, B., Yang, D., Ramsey, S.E., Montealegre Sanchez, G.A., Tenbrock, K., Wittkowski, H., Jones, O.Y., Kuehn, H.S., Lee, C.-C.R., DiMattia,

M.A., Cowen, E.W., Gonzalez, B., Palmer, I., DiGiovanna, J.J., Biancotto, A., Kim, H., Tsai, W.L., Trier, A.M., Huang, Y., Stone, D.L., Hill, S., Kim, H.J., St. Hilaire, C., Gurprasad, S., Plass, N., Chapelle, D., Horkayne-Szakaly, I., Foell, D., Barysenka, A., Candotti, F., Holland, S.M., Hughes, J.D., Mehmet, H., Issekutz, A.C., Raffeld, M., McElwee, J., Fontana, J.R., Minniti, C.P., Moir, S., Kastner, D.L., Gadina, M., Steven, A.C., Wingfield, P.T., Brooks, S.R., Rosenzweig, S.D., Fleisher, T.A., Deng, Z., Boehm, M., Paller, A.S., Goldbach-Mansky, R., 2014. Activated STING in a Vascular and Pulmonary Syndrome. N Engl J Med 371, 507–518. https://doi.org/10.1056/NEJMoa1312625

33. Lu, D., Shang, G., Li, J., Lu, Y., Bai, X., Zhang, X., 2022. Activation of STING by targeting a pocket in the transmembrane domain. Nature 604, 557–562. https://doi.org/10.1038/s41586-022-04559-7
34. Maekawa, H., Inoue, T., Ouchi, H., Jao, T.-M., Inoue, R., Nishi, H., Fujii, R., Ishidate, F., Tanaka, T., Tanaka, Y., Hirokawa, N., Nangaku, M., Inagi, R., 2019. Mitochondrial Damage Causes Inflammation via cGAS-STING Signaling in Acute Kidney Injury. Cell Reports 29, 1261-1273.e6. https://doi.org/10.1016/j.celrep.2019.09.050
35. Maelfait, J., Bridgeman, A., Benlahrech, A., Cursi, C., Rehwinkel, J., 2016. Restriction by SAMHD1 Limits cGAS/STING-Dependent Innate and Adaptive Immune Responses to HIV-1. Cell Reports 16, 1492–1501. https://doi.org/10.1016/j.celrep.2016.07.002
36. Mankan, A.K., Schmidt, T., Chauhan, D., Goldeck, M., Höning, K., Gaidt, M., Kubarenko, A.V., Andreeva, L., Hopfner, K.-P., Hornung, V., 2014. Cytosolic RNA:DNA hybrids activate the cGAS-STING axis. EMBO J 33, 2937–2946. https://doi.org/10.15252/embj.201488726
37. Melki, I., Rose, Y., Uggenti, C., Eyck, L.V., Frémond, M.-L., Kitabayashi, N., Rice, G.I., Jenkinson, E.M., Boulai, A., Jeremiah, N., Gattorno, M., Volpi, S., Sacco, O., Terheggen-Lagro, S.W.J., Tiddens, H.A.W.M., Meyts, I., Morren, M.-A., Haes, P.D., Wouters, C., Legius, E., Corveleyn, A., Rieux-Laucat, F., Bodemer, C., Callebaut, I., Rodero, M.P., Crow, Y.J., 2017. Disease-associated mutations identify a novel region in human STING necessary for the control of type I interferon signaling. Journal of Allergy and Clinical Immunology 140, 543-552.e5. https://doi.org/10.1016/j.jaci.2016.10.031
38. Morehouse, B.R., Govande, A.A., Millman, A., Keszei, A.F.A., Lowey, B., Ofir, G., Shao, S., Sorek, R., Kranzusch, P.J., 2020. STING cyclic dinucleotide sensing originated in bacteria. Nature 586, 429–433. https://doi.org/10.1038/s41586-020-2719-5
39. Mukai, K., Konno, H., Akiba, T., Uemura, T., Waguri, S., Kobayashi, T., Barber, G.N., Arai, H., Taguchi, T., 2016. Activation of STING requires palmitoylation at the Golgi. Nat Commun 7, 11932. https://doi.org/10.1038/ncomms11932
40. Rehwinkel, J., Gack, M.U., 2020. RIG-I-like receptors: their regulation and roles in RNA sensing. Nat Rev Immunol 20, 537–551. https://doi.org/10.1038/s41577-020-0288-3
41. Ritchie, C., Cordova, A.F., Hess, G.T., Bassik, M.C., Li, L., 2019. SLC19A1 Is an Importer of the Immunotransmitter cGAMP. Molecular Cell 75, 372-381.e5. https://doi.org/10.1016/j.molcel.2019.05.006

42. Shang, G., Zhang, C., Chen, Z.J., Bai, X., Zhang, X., 2019. Cryo-EM structures of STING reveal its mechanism of activation by cyclic GMP–AMP. Nature 567, 389–393. https://doi.org/10.1038/s41586-019-0998-5
43. Sharma, S., Schattgen, S., Chan, J., Huyler, A., Rothstein, A., Fitzgerald, K., 2013. The role of innate immune adaptor STING in suppressing lupus (P4070). The Journal of Immunology 190.
44. Sliter, D.A., Martinez, J., Hao, L., Chen, X., Sun, N., Fischer, T.D., Burman, J.L., Li, Y., Zhang, Z., Narendra, D.P., Cai, H., Borsche, M., Klein, C., Youle, R.J., 2018. Parkin and PINK1 mitigate STING-induced inflammation. Nature 561, 258–262. https://doi.org/10.1038/s41586-018-0448-9
45. Srikanth, S., Woo, J.S., Wu, B., El-Sherbiny, Y.M., Leung, J., Chupradit, K., Rice, L., Seo, G.J., Calmettes, G., Ramakrishna, C., Cantin, E., An, D.S., Sun, R., Wu, T.-T., Jung, J.U., Savic, S., Gwack, Y., 2019. The Ca2+ sensor STIM1 regulates the type I interferon response by retaining the signaling adaptor STING at the endoplasmic reticulum. Nat Immunol 20, 152–162. https://doi.org/10.1038/s41590-018-0287-8
46. Sun, L., Wu, J., Du, F., Chen, X., Chen, Z.J., 2013. Cyclic GMP-AMP Synthase Is a Cytosolic DNA Sensor That Activates the Type I Interferon Pathway. Science 339, 786–791. https://doi.org/10.1126/science.1232458
47. Vinogradova, E.V., Zhang, X., Remillard, D., Lazar, D.C., Suciu, R.M., Wang, Y., Bianco, G., Yamashita, Y., Crowley, V.M., Schafroth, M.A., Yokoyama, M., Konrad, D.B., Lum, K.M., Simon, G.M., Kemper, E.K., Lazear, M.R., Yin, S., Blewett, M.M., Dix, M.M., Nguyen, N., Shokhirev, M.N., Chin, E.N., Lairson, L.L., Melillo, B., Schreiber, S.L., Forli, S., Teijaro, J.R., Cravatt, B.F., 2020. An Activity-Guided Map of Electrophile-Cysteine Interactions in Primary Human T Cells. Cell 182, 1009-1026.e29. https://doi.org/10.1016/j.cell.2020.07.001
48. Wang, Y., Wang, F., Zhang, X., 2021. STING-associated vasculopathy with onset in infancy: a familial case series report and literature review. Ann Transl Med 9, 176. https://doi.org/10.21037/atm-20-6198
49. Wang, Z., Chen, J., Hu, J., Zhang, H., Xu, F., He, W., Wang, X., Li, M., Lu, W., Zeng, G., Zhou, P., Huang, P., Chen, S., Li, W., Xia, L., Xia, X., 2019. cGAS/STING axis mediates a topoisomerase II inhibitor–induced tumor immunogenicity. J Clin Invest 129, 4850–4862. https://doi.org/10.1172/JCI127471
50. Yu, X., Zhang, L., Shen, J., Zhai, Y., Jiang, Q., Yi, M., Deng, X., Ruan, Z., Fang, R., Chen, Z., Ning, X., Jiang, Z., 2021. The STING phase-separator suppresses innate immune signalling. Nat Cell Biol 23, 330–340. https://doi.org/10.1038/s41556-021-00659-0
51. Zhang, B., Nandakumar, R., Reinert, L.S., Huang, J., Laustsen, A., Gao, Z., Sun, C., Jensen, S.B., Troldborg, A., Assil, S., Berthelsen, M.F., Scavenius, C., Zhang, Y., Windross, S.J., Olagnier, D., Prabakaran, T., Bodda, C., Narita, R., Cai, Y., Zhang, C., Stenmark, H., Doucet, C.M., Noda, T., Guo, Z., Goldbach-Mansky, R., Hartmann, R., Chen, Z.J., Enghild, J.J., Bak, R.O., Thomsen, M.K., Paludan, S.R., 2020. STEEP mediates STING ER exit and activation of signaling. Nat Immunol 21, 868–879. https://doi.org/10.1038/s41590-020-0730-5
52. Zhang, C., Shang, G., Gui, X., Zhang, X., Bai, X., Chen, Z.J., 2019. Structural basis of STING binding with and phosphorylation by TBK1. Nature 567, 394–398. https://doi.org/10.1038/s41586-019-1000-2

53. Zhao, B., Du, F., Xu, P., Shu, C., Sankaran, B., Bell, S.L., Liu, M., Lei, Y., Gao, X., Fu, X., Zhu, F., Liu, Y., Laganowsky, A., Zheng, X., Ji, J.-Y., West, A.P., Watson, R.O., Li, P., 2019. A conserved PLPLRT/SD motif of STING mediates the recruitment and activation of TBK1. Nature 569, 718–722. https://doi.org/10.1038/s41586-019-1228-x
54. Zhao, B., Shu, C., Gao, X., Sankaran, B., Du, F., Shelton, C.L., Herr, A.B., Ji, J.-Y., Li, P., 2016. Structural basis for concerted recruitment and activation of IRF-3 by innate immune adaptor proteins. Proceedings of the National Academy of Sciences 113, E3403–E3412. https://doi.org/10.1073/pnas.1603269113
55. Zhao, Q., Wei, Y., Pandol, S.J., Li, L., Habtezion, A., 2018. STING Signaling Promotes Inflammation in Experimental Acute Pancreatitis. Gastroenterology 154, 1822-1835.e2. https://doi.org/10.1053/j.gastro.2018.01.065

Key Resources Table

Resource or Reagent	Description	Source and/or Reference	ID
Recombinant DNA			
pcDNA3-hSTING-HA		(Ergun et al., 2019)	N/A
pcDNA-hSTING-C148A		(Ergun et al., 2019)	N/A
pcDNA3-hSTINGΔCTT-HA		(Ergun et al., 2019)	N/A
pcDNA3-hSTINGΔCTT-R281E-HA		This paper	N/A
pcDNA3-hSTINGΔCTT-R284E-HA		This paper	N/A
pcDNA3-hSTINGΔCTT-Q273A/A277Q-HA		This paper	N/A
pcDNA3-CTT1-FLAG (hSTING340–353)		This paper	N/A
pcDNA3-CTT2-FLAG (hSTING354–366)		This paper	N/A
pcDNA3-CTT3-FLAG (hSTING367–379)		This paper	N/A
pcDNA3-CTT3-FLAG-E369R (hSTING367–379)		This paper	N/A
pcDNA3-CTT7 (hSTING 368–374)		This paper	N/A
pcDNA3-nCTT7 (hSTING 373–379)		This paper	N/A
pTB146 hSTING-CTD (aa 137–366)		This paper	N/A
Str-Ii-SBP-hSTING-FLAG (RUSH)		This paper	N/A
pcDNA3-hSTING-C29S-HA		This paper	N/A
pcDNA3-hSTING-C64S-HA		This paper	N/A
pcDNA3-hSTING-C91S-HA		This paper	N/A
pcDNA3-hSTING-C88/91S-HA		This paper	N/A
pcDNA3-hSTING-C12/29/64/88/91S-HA (5C5S)		This paper	N/A
cDNA3-hSTING-C12/29/88/91S-HA (5C5S+64)		This paper	N/A

cDNA3-hSTING-C12/29/64/88S-HA (5C5S+91)		This paper	N/A
cDNA3-hSTING-C12/29/88S-HA (5C5S+64,91)		This paper	N/A
cDNA3-TBK1-FLAG		Genscript	Cat#: OHu15095D
Chemicals, reagents and peptides			
Phusion High-Fidelity DNA polymerase		NEB	Cat #: M0530S
dNTPs		NEB	Cat #: N0447S
Phusion GC Buffer		NEB	Cat #: B0519
Gibson Assembly HiFi DNA Master Mix		NEB	Cat #: E2621
Pfu Turbo DNA polymerase		Agilent	Cat #: 600250
Protein A Magnetic Beads		Cell Signaling Technologies	Cat #: 73778S
Protein A Agarose Beads		ThermoFisher	Cat #: 20333
Prolong Diamond Antifade Mountant		ThermoFisher	Cat #: P36961
DAPI		ThermoFisher	Cat # D3571
DpnI		NEB	Cat #: R0176S
HisPur Cobalt Resin		ThermoFisher	Cat #: 89966
ZymoPure Plasmid Miniprep Kit		Zymo Research	Cat #: D4212
ZymoClean Gel DNA Recovery		Zymo Research	Cat #: D4002
Direct-zol RNA extraction kit		Zymo Research	Cat #: R2050
cOmplete protease inhibitor tablets		Roche	Cat #: 11697498001
2’,3’-cGAMP	In-house synthesis	(Ritchie et al., 2019)	N/A
H-151	In-house synthesis	(Haag et al., 2018)	N/A
H-151AL	In-house synthesis	(Haag et al., 2018)	N/A
Peptide H_2N–MEKPLPL–CO_2H		Genscript	N/A
Peptide CTT1 H_2N–EVTVGSLKTSAVP-CO_2H		Stanford Protein and Nucleic Acid Facility	N/A

Peptide CTT2 H_2N–STSTMSQEPELLIS-CO_2H		Stanford Protein and Nucleic Acid Facility	N/A
Peptide CTT3 H_2N–GMEKPLPLRTDFS-CO_2H		Stanford Protein and Nucleic Acid Facility	N/A
17-Octadecynoic Acid		Cayman Chemical	Item #: 90270
IRdye 800CW Azide Infrared Dye		LI-Cor Biosciences	P/N: 929-60000
AccuPower 2X Greenstar qPCR Master Mix		Bioneer	Cat #: K-6251
L-methionine-N-FMOC (^{15}N, 98%)		Cambridge Isotope Laboratories, Inc.	Cat #: NLM-4632-PK
L-leucine-N-FMOC (^{15}N, 98%)		Cambridge Isotope Laboratories, Inc.	Cat #: NLM-2397-PK
L-lysine-alpha-N-FMOC ($^{15}N_2$, 96-98%)		Cambridge Isotope Laboratories, Inc.	Cat #: NLM-4631-0.1
L-proline-N-FMOC (^{15}N, 98%)		Cambridge Isotope Laboratories, Inc.	Cat #: NLM-3906-0.25
L-glutamic acid-N-FMOC, gamma-tert-butyl ester (^{15}N, 98%)		Cambridge Isotope Laboratories, Inc.	Cat #: NLM-8960-0.1
Antibodies			
α-tubulin (DM1A), Mouse mAb		Sigma-Aldrich	Cat#: T6199; RRID:AB_477583
STING (D2P2F) Rabbit mAb		Cell Signaling Technologies	Cat#: 13647; RRID: AB_2732796
HA-Tag (C29F4) Rabbit mAb		Cell Signaling Technologies	Cat#: 3724; RRID: AB_1549585
DYKDDDDK (D6W5B) Rabbit mAb		Cell Signaling Technologies	Cat#: 14793 RRID:AB_2572291
Phospho-IRF-3 (Ser396) (D6O1M) Rabbit mAb		Cell Signaling Technologies	Cat# 10327; RRID: AB_2773013
IRF-3 (D83B9) Rabbit mAb		Cell Signaling Technologies	Cat# 4302; RRID: AB_1904036
Phospho-TBK1/NAK (Ser172) (D52C2) Rabbit mAb		Cell Signaling Technologies	Cat# 5483; RRID: AB_10693472
TBK1/NAK (E8I3G) Rabbit mAb		Cell Signaling Technologies	Cat#: 38066; RRID:AB_2827657

Sheep anti-human TGN46		Bio-Rad	Cat#: AHP500GT
DYKDDDDK (9A3) Mouse mAb		Cell Signaling Technologies	Cat#: 8146
Donkey anti-Sheep IgG (H+L) Cross-Adsorbed Secondary Antibody, Alexa Fluor 647		Life Technologies Corporation	Cat #: A21448
Anti-mouse IgG (H+L), F(ab')2 Fragment (Alexa Fluor® 488 Conjugate)		Cell Signaling Technologies	Cat #: 4408
Goat Anti-Mouse IgG Antibody, IRDye® 680RD Conjugated		Li-COR Biosciences	Cat# 926-68070; RRID: AB_10956588
IRDye 800CW Goat anti-Rabbit IgG (H+L)		Li-COR Biosciences	Cat# 925-32211; RRID: AB_2651167
Critical Commercial Assays			
QUANTI-Luc		Invivogen	Cat #: rep-qlc2
Software and algorithms			
PyMOL		The PyMOL Molecular Graphics System, Version 2.5.2., Schrodinger, LLC	https://pymol.org/2/
Maestro		Schrodinger	https://www.schrodinger.com/products/maestro
GraphPad Prism 9		GraphPad Software	https://www.graphpad.com/
Image Studio Lite		LI-COR	https://www.licor.com/bio/image-studio/
Other			
Amicon Ultra-0.5 centrifugal filter unit		Merck	Cat#: UFC500396
Amicon concentrators (3 K)		Millipore	Cat#: UFC800308
Amicon concentrators (10 K)		Millipore	Cat#: UFC901096
Amicon concentrators (30 K)		Millipore	Cat#: UFC903024
HiTrap Q Sepharose FF (5 mL)		GE Healthcare	Cat#: 17-5156-01
Superdex 200 increase 10/300 GL		GE Healthcare	Cat#: 17517501
Bacterial strains			
E. coli Rosetta(DE3) cells		Sigma-Aldrich	Cat#: 79054

E. coli XL1-Blue cells		Agilent	Cat#: 200249
Mammalian cell lines			
HEK293T Dual-Null		Invivogen	Cat#: 293d-null
HEK293 T		ATCC	ATCC CRL-3216; RRID: CVCL_0063
U937		ATCC	ATCC ATCC CRL-1593.2; RRID: CVCL_0007
THP-1		ATCC	ATCC TIB-202; RRID: CVCL_0006
HeLa		ATCC	ATCC CCL-2; RRID: CVCL_0030
Jurkat		ATCC	ATCC TIB-152; RRID:CVCL_036
Biological Samples			
Buffy coat from donors		Stanford Blood Center	N/A

Material Availability
Further information and requests for reagents should be directed to and will be fulfilled by the lead contact, Lingyin Li (lingyinl@ stanford.edu or lingyin@arcinstitute.org).

Methods
Cloning
Unless otherwise stated in subsequent sections, pcDNA-STING plasmids containing point mutations were made by modifying the previously reported wild-type pcDNA-STING plasmid by site-directed mutagenesis using the QuikChange protocol with the indicated primers, followed by Dpn1-digestion. All recombinant plasmids were transformed into XL1-Blue competent cells (Agilent) and sequenced for verification.

Experimental Models and Subject Details
Human peripheral blood mononuclear cells (PBMCs) were isolated from whole blood using standard Ficoll procedures and were cultured in RPMI (Corning Cellgro) supplemented with 2% human AB serum (Corning) and 100 U/mL penicillin-streptomycin (ThermoFisher). Buffy coat samples from whole blood were obtained de-identified from the Stanford Blood Center so no sex, gender-identify, or age is associated with the sample.

HEK293T, 293T-Dual Null and HeLa Kyoto cells were cultured in DMEM (Gibco) supplemented with 10% FBS (Atlanta Biologics) (v/v) and 100 U/mL penicillin-streptomycin (Gibco) and maintained in 37ºC incubators with 5% CO_2. U937, THP-1 and Jurkat cells were cultured similarly except in RPMI (Gibco) supplemented with 10% heat-inactivated FBS (Atlanta Biologics) (v/v) and 100 U/mL penicillin-streptomycin (Gibco).

Cell stimulation
HEK293T cells were plated in a 12-well plate at 300,000 cells/well. After 24h, they were transfected with indicated plasmids using FuGENE 6 transfection reagent (Promega). After another 24h, 2'3'-cGAMP was added to the media at 100μM. For RUSH experiments, biotin was added alone or concurrently with cGAMP at 40μM. For experiments containing C91-reactive compounds, the cells were pre-treated with these ligands at indicated concentrations for 2h prior to cGAMP stimulation. After 2h cGAMP stimulation, cells were lysed directly on the plate in 2x Laemmli sample buffer (LSB) or non-reducing SDS buffer (Laemmli sample buffer lacking BME) and STING activation was measured by western blot. U937, Hela Kyoto, THP-1, Jurkats, and PBMCs were all stimulated similarly.

Western Blot
Lysates prepared as described in respective protocols were separated on a SurePage Bis-Tris polyacrylamide gel (Genscript) and transferred to a nitrocellulose membrane using the semi-dry iBlot2 system (Invitrogen). The membrane was blocked for 1 h at room temperature (Intercept blocking buffer, Li-COR Biosciences), and incubated with relevant primary antibodies overnight at 4ºC. Following three washes in 1xTBS-0.1% tween, secondary antibody (Anti-rabbit, anti-mouse, Li-Cor Biosciences) was added for 1 h at room temperature, followed by three additional washes in TBS-T. Blots were imaged in IR using a Li-Cor Odyssey Blot Imager.

17-ODYA labeling and click-immunoprecipitation
Cells were transfected with corresponding plasmids as above. 24h following transfection, cells were changed into low-serum DMEM (2% FBS) containing 60μM 17-ODYA for 3.5h total, with the addition of 100μM 1.5h into this labeling. After labeling and cGAMP stimulation. The cells were washed in cold PBS, then harvested. Cell pellets were lysed in modified RIPA buffer (150mM NaCl, 4% SDS, 50mM triethanolamine (TEA) pH 7.4) with protease inhibitors by incubating on rotation at 4C for 30m. Lysate was cleared at 14000rpm for 15m. Cleared lysate was then diluted five-fold in TEA lysis buffer (1% Triton X-100, 150mM NaCl, 50mM TEA pH 7.4) and incubated with prewashed Protein A agarose beads and anti-HA or anti-FLAG antibody on rotation at 4C overnight. The following day, the beads were washed 3x in TEA lysis buffer. Proteins bound to beads were conjugated to IRdye800-azide in 50μl PBS with click chemistry reactants for 2h at 37ºC with constant agitation. Click chemistry reactants were freshly prepared as a 5X master mix that consists of 0.5mM IRdye800-azide, 15mM BTTAA, 25mM sodium ascorbate, and 50mM $CuSO_4 \cdot 5H_2O$. Beads were then washed 3x in modified RIPA buffer and proteins were eluted by boiling in 1X Laemmli sample buffer (diluted in modified RIPA) and subsequently resolved by SDS-PAGE.

Vesicle isolation
HEK293T cells were plated at 4M cells/ dish in 10 cm dishes. The following day, the cells were transfected with full-length STING. The following day, cells were treated with 200μM cGAMP for 10m and then washed in ice cold PBS. The cells were then incubated in ice cold PBS for 5m and then washed in hypotonic lysis buffer (25mM Tris-HCl, pH 7.5, 50mM sucrose, 0.5mM MgCl2, 0.2mM EGTA) and then incubated 5m in the same buffer. The

plates were then stood vertically for 1 m to remove excess buffer. The cells were then lysed in 2 mL hypotonic lysis buffer with protease inhibitor added. The cells were scraped from the plate and passed through a 20G syringe 30x. Immediately following lysis the hypotonic buffer was neutralized through addition of hypertonic buffer (2.5M sucrose, 25mM Tris-HCl pH 7.5, 0.5mM MgCl2, 0.2mM EGTA). The lysate was spun 1000xg for 10m. The supernatant was collected and re-spun at 78,000xg. The supernatant was again collected and spun at 238,000xg to collect the vesicles. The pellet was collected, lysed in 2% DDM and run on native page to measure STING oligomerization state.

IFN-β Reporter Assay

HEK293T cells stably expressing a secreted IFNβ-luciferase reporter (Invivogen) were transfected with indicated plasmids. After 24h, cells were stimulated with 100μM cGAMP. After an additional 20h, luciferase activity was measured using the Quanti-Luc system (Invivogen).

Co-immunoprecipitation

Co-immunoprecipitation experiments were performed as previously described. Briefly, HEK293T were plated and transfected as described above (see Cell Stimulation). For CTT pulldown experiments, transfection was performed with 100 ng pcDNA3-hSTING or a variant and 600 ng pcDNA3-FLAG expressing a CTT fragment. After 20 h, the cells were lysed in 300 μL hypotonic lysis buffer supplemented with protease inhibitor tablet (Roche, see Vesicle isolation). The lysates were split into two and half was treated with cGAMP. Primary anti-rabbit FLAG antibody (Cell Signaling Technologies) was added (1:50) overnight. Lysates were incubated with Protein A beads pre-washed in lysis buffer for 30 min at room temperature and washed 5 times in hypotonic lysis buffer supplemented with 0.1% DDM buffer. Protein was eluted from beads in 1xLSB and boiled 10 min at 95ºC. Protein was analyzed with western blotting. For STING-TKB1 pulldown experiments, co-immunoprecipitation was done as previously described in Zhang et al Nature (2019).

Blue-Native PAGE

Cells were lysed in native lysis buffer (10% glycerol, 25mM NaCl, 20mM HEPES pH 7.0) + 1% DDM and protease inhibitor (Roche) and solubilized by rotating 30m at 4C. Lysates were spun for 15 m at 14000 rpm and supernatant was collected. Lysate was added to 4x native sample buffer (Invitrogen), run on a NativePAGE gel (Invitrogen), and transferred to a PVDF membrane using either a wet transfer system (BioRad) or semi-dry iBlot transfer system (ThermoFisher). Western blotting protocol was followed for membrane staining.

Confocal microscopy

HeLa Kyoto cells were plated on glass coverslips and after 24 hours, then transfected and stimulated as described above. Cells were washed once in cold PBS, then fixed for 20 minutes in 4% paraformaldehyde in PBS. They were then permeabilized for 10 minutes in 0.1% Triton-X in PBS (PBS-T), and blocked in 3% BSA in PBS-T for 30 minutes. Primary (Anti-HA, rabbit) was added 1:800 in blocking buffer for 1 hour. Cells were then washed in PBS-T and secondary (A647 anti-sheep 1:2000, A488 anti-mouse 1:1000).

Coverslips were mounted on slides using Prolong Diamond Antifade Mountant (ThermoFisher) and allowed to cure for 24 hours. Slides were imaged on both a Leica DM16000 inverted spinning disk confocal microscope as well as a Zeiss LSM Airyscan 980 confocal microscope.

Cysteine reactivity profiling

Profile of STING cysteine reactivity was performed using established workflows (Cravatt et al., 2023; Vinogradova et al., 2020). THP-1 cells were treated with either DMSO, 20μM WX-03-59, WX-03-60 or co-treated with 100μM cGAMP for 3h. Whole native lysates were then chased with iodoacetamide desthiobiotin (IA-DTB). IA-DTB labeled peptides were enriched with streptavidin beads after trypsin digestion and analyzed by MS3 following TMT16plex tagging.

Protein expression and purification

His-tagged STING CTDs were purified as previously described (Ergun 2019). Briefly, Rosetta competent cells transformed with pTB146 vector expressing hSTING CTD lacking CTT3 (hSTING aa 137–366) were grown in 2XYT media with 100 ng/mL ampicillin. Cells were induced at OD 1 with 0.5 mM IPTG and grown overnight at 16ºC. Cells were pelleted, resuspended in TBS pH 8, and snap-frozen in liquid nitrogen. Cells were lysed with two freeze thaw cycles, followed by sonication (4 x 30 s at 35% power). Cell debris was removed by ultracentrifugation for 45 minutes at 40,000g. The supernatant was incubated with HisPur cobalt resin (ThermoFisher) for 1 h at 4ºC. The beads were washed in 20 mM imidazole in TBS and eluted in 300 mM imidazole. The hisSUMO tag was cleaved overnight at 4ºC by Ulp1 (1:1000 molar ratio), and the tag and His-Ulp1 were removed using cobalt resin. Protein was further purified using size-exclusion chromatography on a Superdex 200 Increase 10/300 GL column (GE Healthcare) using an Akta pure system (GE Healthcare) with TBS pH 8 as the running buffer. Fractions containing protein were verified by SDS-PAGE with Coomassie staining and pooled. The protein was concentrated to 10 mg/mL using Amicon 10K concentrators, aliquoted, snap-frozen in liquid nitrogen and stored at -80ºC prior to use.

cGAMP Binding Assay

cGAMP binding was verified using the radioactivity-based nitrocellulose filter binding assay as previously described (Li et al., 2014). ^{32}P-labeled cGAMP was mixed with 100 μM STING CTD and stoichiometric amounts of small molecule competitors (cold cGAMP, CTT1, CTT2 or CTT3, all 10 mM solutions in water). The mixture was loaded into an Amicon Ultra-0.5 centrifugal filter unit and centrifuged at 12,000g for 10 min. For each sample, 5 μL of flowthrough was mixed with 10 mL of scintillation fluid (Research Products International) and readout was performed on a Beckman Coulter LS6500 Liquid Scintillation Counter.

Synthesis of ^{15}N-labelled CTT7

^{15}N isotopically labelled, Fmoc-protected amino acids were obtained from Cambridge Isotope Laboratories and used without further modification. Peptide synthesis was performed on a CSBio CS336X instrument using standard Fmoc-based solid-phase peptide synthesis. 25 μmol Rink amide AM resin (CSBio) was used to initiate the

synthesis, with each coupling step performed with 0.1 mmol of protected amino acid for 3 h at room temperature in the presence of HBTU and N,N-diisopropylethylamine (DIEA). Peptide cleavage and removal of the ester protecting group of glutamic acid was performed by stirring the resin in 95% trifluoroacetic acid (TFA), 2.5% water and 2.5% triisopropylsilane for 4 h at room temperature. The peptide was precipitated in ice-cold diethyl ether and collected by centrifugation at 4000*g* for 15 min. The solid was washed twice with cold diethyl ether, then dried over a stream of dry nitrogen gas and redissolved in HPLC-grade water. Purification was performed via high-performance liquid chromatography (HPLC) on a C18 semi-prep column using a water–acetonitrile gradient in the presence of 0.1% trifluoroacetic acid. Fractions were tested by ESI-MS to verify the correct mass of product, collected, pooled and lyophilized.

NMR experiments

^{15}N-labelled CTT7 prepared as described above was dissolved in D_2O and reconstituted to 1.5 mM in 1.1x TBS such that the overall solution contained 10% deuterated solvent for signal locking. In samples containing STING, TBS was replaced with buffer containing STING CTD purified as described above and concentrated to 1.5 mM, with the appropriate addition of unlabelled CTT7 (Genscript) or 2',3'-cGAMP (synthesized in-house according to Ritchie et al., 2019). NMR data were collected on an Varian Inova 600 MHz NMR Spectrometer with a 5 mm room temperature HCN probe. ^{15}N–^{1}H HSQC data were collected at 25ºC using the gNhsqc pulse sequence with 2 scans for 0.085 seconds over 12000 Hz with 2048 complex points in ^{1}H dimension, and 200 complex points over 1000 Hz in the ^{15}N dimension.

Computational modeling of STING–CTT interaction

A monomer of wild-type apo STING C-terminal domain (PDB: 4F5W) was isolated and minimized in Schrödinger Maestro using standard protein preparation workflow using all default settings at pH 7.4, with missing side chains filled against the corresponding FASTA sequence and using the OPLS3e force field. The molecule CTT7 was constructed from a structure file and optimized for all protonation states and stable conformations at pH 7.4 using the LigPrep workflow. Binding site prediction was run and a site containing the residues R284, R281, D320 and Q315 was selected and used to generate a receptor grid suitable for peptide docking (all other default parameters). The receptor grid was used to dock all prepared conformations of CTT using Glide at standard precision.

Quantitative PCR

Human PBMCs were treated with cGAMP for 16 h. Cells were then lysed and total RNA was extracted using Direct-zol RNA extraction kit (Zymo) following manufacturer protocols. RNA was reverse transcribed in 20 mL reactions containing 500 ng total RNA, 100 pmol Random Hexamer Primers (Thermo Scientific), 0.5 mM dNTPs (NEB), 20 U RNaseOUT (Invitrogen), 1x Maxima RT Buffer (Thermo Scientific), and 200 U Maxima Reverse Transcriptase (Thermo Scientific). Reverse transcription reactions were incubated first for 10 min at 37ºC, then for 30 min at 50ºC. Reactions were then terminated by incubating for 5 min at 85ºC. To quantify transcript levels, 10 mL reactions were set up containing 1x GreenStar Master Mix (Bioneer), 10x ROX dye (Bioneer), 100 nM forward and reverse primers, and 0.7 mL of reverse transcription reactions. To determine Ct

values, reactions were run on a Roche Lightcycler 480 II. using the following program: ramp up to 50ºC (1.6ºC/s) and incubate for 2 min, ramp up to 95ºC (1.6ºC/s) and incubate for 10 min; then 40 cycles of ramp up to 95ºC (1.6ºC/s) and incubate for 15 s, ramp down to 60ºC (1.6ºC/s) and incubate for 1 min. Primer sequences are provided in Table S1.

Table S1: Oligonucleotide sequences used in this study

Name	Description	Sequence (5' → 3')
hSTING Q196A	Quikchange Primer (Forward)	CGGGGTGCAGTGAGCGCACGGCTGTATATTCTCCTCCC
hSTING Q196A	Quikchange Primer (Reverse)	GGGAGGAGAATATACAGCCGTGCGCTCACTGCACCCCG
hSTING N183A	Quikchange Primer (Forward)	GCCCGGATTCGAACTTACGCACAGCATTACAACAACC
hSTING N183A	Quikchange Primer (Reverse)	GGTTGTTGTAATGCTGTGCGTAAGTTCGAATCCGGGC
hSTING L172A	Quikchange Primer (Forward)	GGATATCTGCGGCTGATCGCACCAGAGCTCCAGGCC
hSTING L172A	Quikchange Primer (Reverse)	GGCCTGGAGCTCTGGTGCGATCAGCCGCAGATATCC
hSTING Y164A	Quikchange Primer (Forward)	CTGGCATGGTCATATGCAATCGGATATCTGCGG
hSTING Y164A	Quikchange Primer (Reverse)	CCGCAGATATCCGATTGCATATGACCATGCCAG
hSTING R197A	Quikchange Primer (Forward)	CGGGGTGCAGTGAGCCAGGCACTGTATATTCTCCTCCC
hSTING R197A	Quikchange Primer (Reverse)	GGGAGGAGAATATACAGTGCCTGGCTCACTGCACCCCG
hSTING R191A	Quikchange Primer (Forward)	GCATTACAACAACCTGCTAGCAGGTGCAGTGAGCCAGCGG
hSTING R191A	Quikchange Primer (Reverse)	CCGCTGGCTCACTGCACCTGCTAGCAGGTTGTTGTAATGC
hSTING M214A	Quikchange Primer (Forward)	GGTGCCTGATAACCTGAGTGCAGCTGACCCCAACATTCG
hSTING M214A	Quikchange Primer (Reverse)	CGAATGTTGGGGTCAGCTGCACTCAGGTTATCAGGCACC
hSTING Q315A	Quikchange Primer (Forward)	CCTCATTGCCTACGCAGAACCTGCAGATGACAGC
hSTING Q315A	Quikchange Primer (Reverse)	GCTGTCATCTGCAGGTTCTGCGTAGGCAATGAG

		G
hSTING D216A	Quikchange Primer (Forward)	CCTGATAACCTGAGTATGGCTGCACCCAACATTCGCTTCC
hSTING D216A	Quikchange Primer (Reverse)	GGAAGCGAATGTTGGGTGCAGCCATACTCAGGTTATCAGG
hSTING N218A	Quikchange Primer (Forward)	CCTGAGTATGGCTGACCCCGCAATTCGCTTCCTGGATAAACTGC
hSTING N218A	Quikchange Primer (Reverse)	GCAGTTTATCCAGGAAGCGAATTGCGGGGTCAGCCATACTCAGG
hSTING L247A	Quikchange Primer (Forward)	GCAACAGCATCTATGAGGCACTGGAGAACGGGCAGCGG
hSTING L247A	Quikchange Primer (Reverse)	CCGCTGCCCGTTCTCCAGTGCCTCATAGATGCTGTTGC
hSTING E249A	Quikchange Primer (Forward)	GCATCTATGAGCTTCTGGCAAACGGGCAGCGGGCG
hSTING E249A	Quikchange Primer (Reverse)	CGCCCGCTGCCCGTTTGCCAGAAGCTCATAGATGC
hSTING Q252A	Quikchange Primer (Forward)	CTTCTGGAGAACGGGGCACGGGCGGGCACCTGTGTCC
hSTING Q252A	Quikchange Primer (Reverse)	GGACACAGGTGCCCGCCCGTGCCCCGTTCTCCAGAAG
hSTING K236A	Quikchange Primer (Forward)	GACCGTGCTGGCATCGCAGATCGGGTTTACAGC
hSTING K236A	Quikchange Primer (Reverse)	GCTGTAAACCCGATCTGCGATGCCAGCACGGTC
hSTING E282A	Quikchange Primer (Forward)	CAAGCTGGCTTTAGCCGGGCAGATAGGCTTGAGCAGGCC
hSTING E282A	Quikchange Primer (Reverse)	GGCCTGCTCAAGCCTATCTGCCCGGCTAAAGCCAGCTTG
hSTING E336A	Quikchange Primer (Forward)	CCGGCACCTGCGGCAGGCAGAAAAGGAAGAGGTTACTGTGG
hSTING E336A	Quikchange Primer (Reverse)	CCACAGTAACCTCTTCCTTTTCTGCCTGCCGCAGGTGCCGG
hSTING L325A	Quikchange Primer (Forward)	GCAGATGACAGCAGCTTCTCGGCATCCCAGGAGGTTCTCCGG
hSTING L325A	Quikchange Primer (Reverse)	CCGGAGAACCTCCTGGGATGCCGAGAAGCTGCTGTCATCTGC
hSTING D320A	Quikchange Primer (Forward)	CCTACCAGGAACCTGCAGATGCAAGCAGCTTCTCGCTGTCC

hSTING D320A	Quikchange Primer (Reverse)	GGACAGCGAGAAGCTGCTTGCATCTGCAGGTTCCTGGTAGG
hSTING R310A	Quikchange Primer (Forward)	CTCTTCTGCCGGACACTTGCAGACATCCTGGCAGATGC
hSTING R310A	Quikchange Primer (Reverse)	GCATCTGCCAGGATGTCTGCAAGTGTCCGGCAGAAGAG
hSTING Q306A	Quikchange Primer (Forward)	GCAGATGCCCCTGAGTCTGCAAACAACTGCCGCCTCATTGC
hSTING Q306A	Quikchange Primer (Reverse)	GCAATGAGGCGGCAGTTGTTTGCAGACTCAGGGGCATCTGC
CTT7 MAKPLPL	Quikchange Primer (Forward)	GACCCAAGCTATGGCAAAGCCCCTCCCTC
CTT7 MAKPLPL	Quikchange Primer (Reverse)	GAGGGAGGGGCTTTGCCATAGCTTGGGTC
CTT7 MFEKPLPL	Quikchange Primer (Forward)	GGAGACCCAAGCTATGTTCGAAAAGCCCCTCCCTC
CTT7 MFEKPLPL	Quikchange Primer (Reverse)	GGAGACCCAAGCTATGTTCGAAAAGCCCCTCCCTC
hSTING Q273A	Quikchange Primer (Forward)	GCCATGTCAGCATACAGTC
hSTING Q273A	Quikchange Primer (Reverse)	GACTGTATGCTGACATGGC
hSTING A277Q	Quikchange Primer (Forward)	TACAGTCAACAGGGCTTTAGC
hSTING A277Q	Quikchange Primer (Reverse)	GCTAAAGCCCTGTTGACTGTA
hSTING R281E	Quikchange Primer (Forward)	GTCAAGCTGGCTTTAGCGAGGAGGATAGGCTTGAGC
hSTING R281E	Quikchange Primer (Reverse)	GTCAAGCTGGCTTTAGCGAGGAGGATAGGCTTGAGC
hSTING R284E	Quikchange Primer (Forward)	GCTTTAGCCGGGAGGATGAGCTTGAGCAGGCCA
hSTING R284E	Quikchange Primer (Reverse)	TGGCCTGCTCAAGCTCATCCTCCCGGCTAAAGC
CTT-E369R	Quikchange Primer (Forward)	GGAGAGGGAGGGGCTTTCTCATTCCACTGATGAGGA
CTT-E369R	Quikchange Primer (Reverse)	TCCTCATCAGTGGAATGAGAAAGCCCCTCCCTCTCC
hSTING C91S	Quikchange Primer (Forward)	GCGGAGGGGGCTGCCCAGGCAGG
hSTING C91S	Quikchange Primer (Reverse)	CCTGCCTGGGCAGCCCCCTCCGC

hSTING C88/91S	Quikchange Primer (Forward)	GGACTGTGCGGGCCTCCCTGGGCTCCCCCCTCCGCCGTGG
hSTING C88/91S	Quikchange Primer (Reverse)	CCACGGCGGAGGGGGGAGCCCAGGGAGGCCCGCACAGTCC
hSTING C12S	Quikchange Primer (Forward)	CTGCATCCATCCATCCCGTCTCCCAGGGGTCACGGGGCC
hSTING C12S	Quikchange Primer (Reverse)	GGCCCCGTGACCCCTGGGAGACGGGATGGATGGATGCAG
hSTING C29S	Quikchange Primer (Forward)	CTTGGTTCTGCTGAGTGCCTCCCTGGTGACCCTTTGGG
hSTING C29S	Quikchange Primer (Reverse)	CCCAAAGGGTCACCAGGGAGGCACTCAGCAGAACCAAG
hSTING C64S	Quikchange Primer (Forward)	CTGCTGTTAAACGGGGTCTCCAGCCTGGCTGAGGAGC
hSTING C64S	Quikchange Primer (Reverse)	GCTCCTCAGCCAGGCTGGAGACCCCGTTTAACAGCAG
ACTB FWD	qPCR primer (Forward)	GGCATCCTCACCCTGAAGTA
ACTB REV	qPCR primer (Reverse)	AGAGGCGTACAGGGATAGCA
IFNB FWD	qPCR primer (Forward)	AAACTCATGAGCAGTCTGCA
IFNB REV	qPCR primer (Reverse)	AGGAGATCTTCAGTTTCGGAGG
CXCL10 FWD	qPCR primer (Forward)	TGCCATTCTGATTTGCTGCC
CXCL10 REV	qPCR primer (Reverse)	CGTGGACAAAATTGGCTTGC
IFIT1 FWD	qPCR primer (Forward)	TGGCAGAAGCCCAGACTTAC
IFIT1 REV	qPCR primer (Reverse)	GCGATAGGCAGAGATCGCAT
IFIT2 FWD	qPCR primer (Forward)	AGAACGCCATTGACCCTCTG
IFIT2 REV	qPCR primer (Reverse)	TAAAACTTGGCTGCACTGCG
IFIT3 FWD	qPCR primer (Forward)	TTGGGCAGACTCTCAGATGC
IFIT3 REV	qPCR primer (Reverse)	CATCGCAATTGCCAGTCCAG

Figure 1. Detailing the kinetic landscape of STING signaling post cGAMP addition.

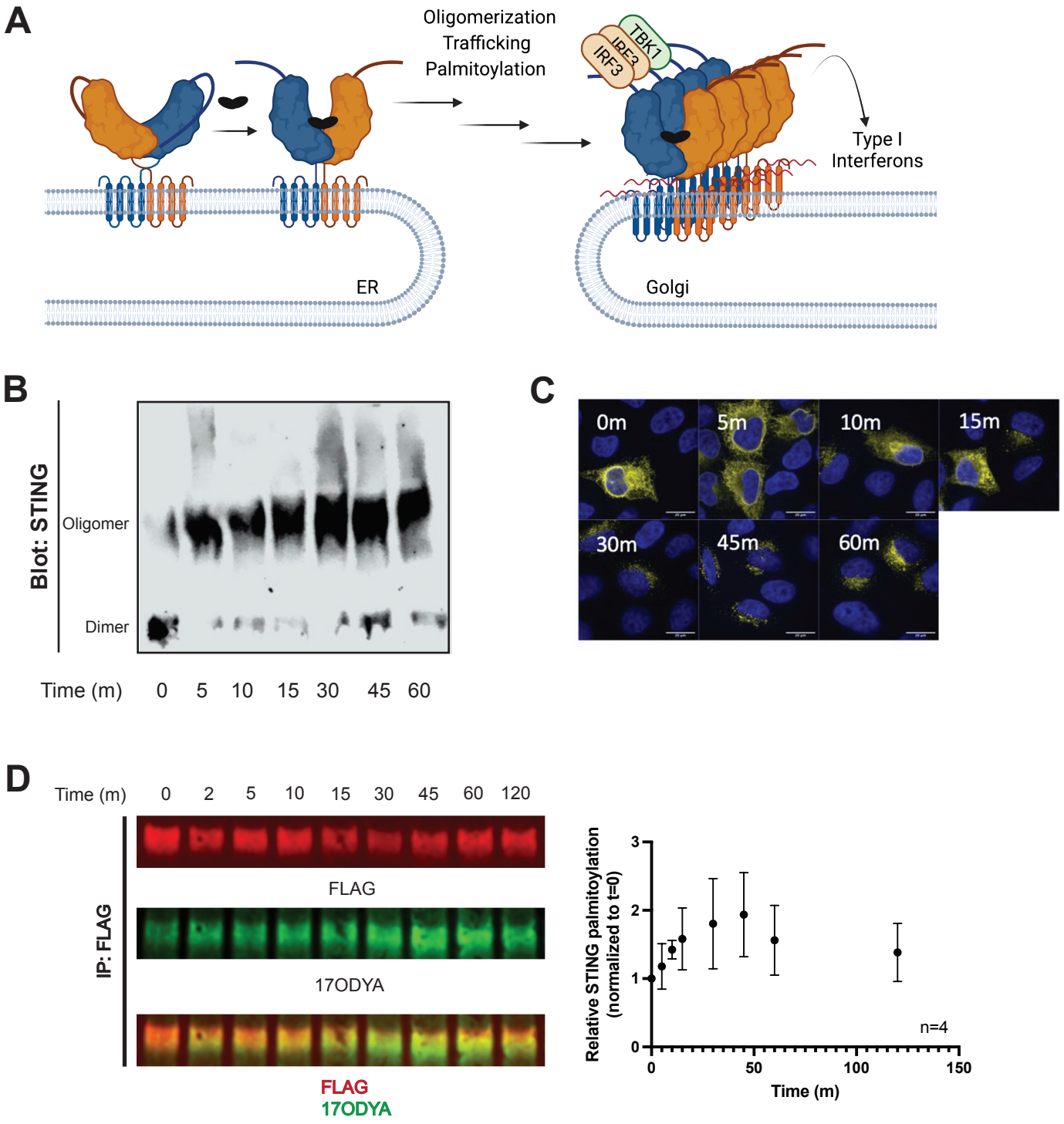

Figure 1. Detailing the kinetic landscape of STING signaling post cGAMP addition. **(A)** Schematic of STING signaling cascade. **(B)** Timecourse of STING oligomerization by BN-PAGE in Hela Kyoto cells expressing STING-HA. **(C)** Timecourse of STING trafficking by confocal microscopy in Hela Kyoto cells expressing STING-HA. **(D)** STING palmitoylation of STING-HA expressing cells overtime post-cGAMP addition. Quantification is depicted as relative STING palmitoylation (17-ODYA relative to STING signal), normalized to relative value at time 0 for each experiment.

Figure 2. Trafficking is not necessary or sufficient for STING activation.

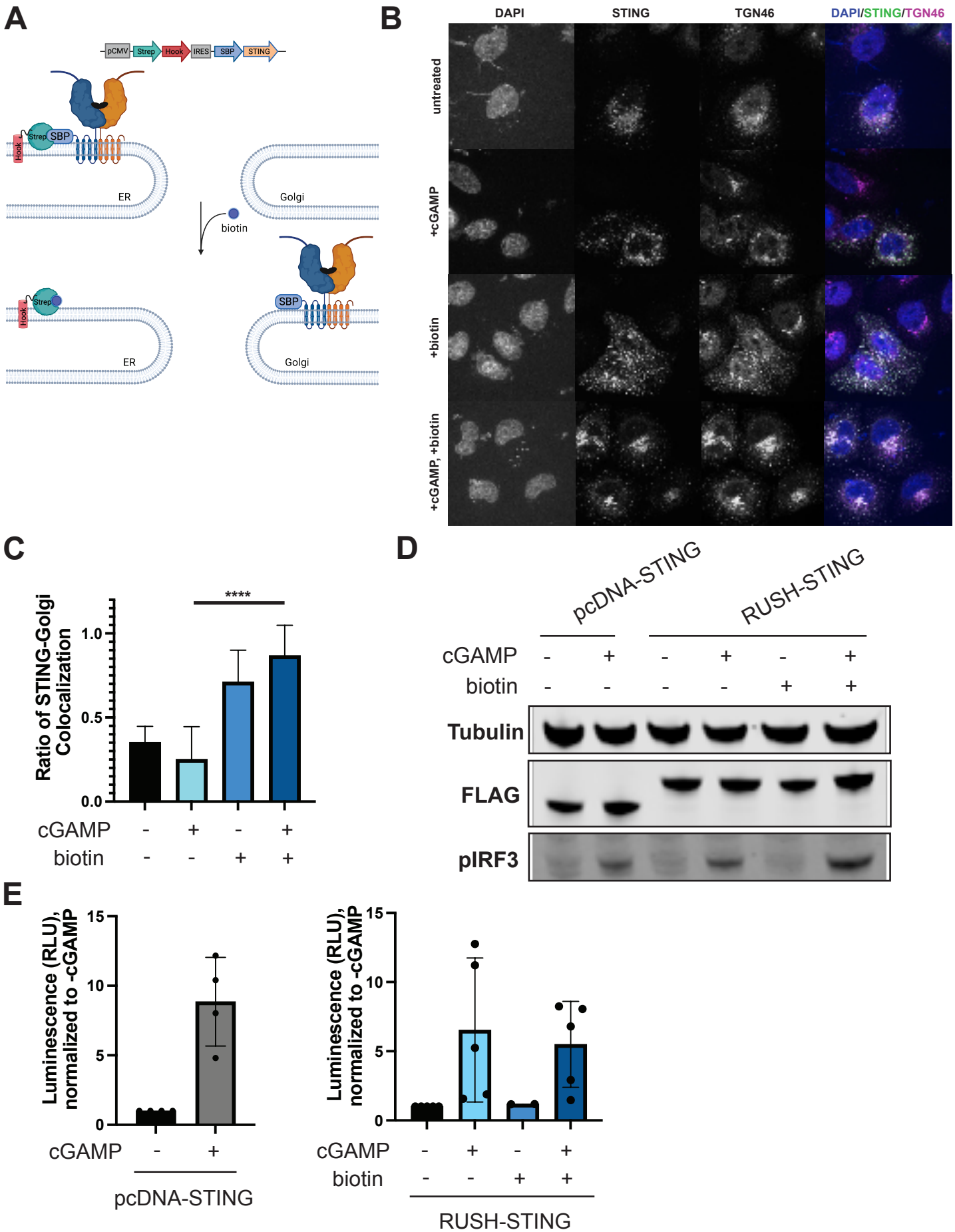

Figure 2. Trafficking is not necessary or sufficient for STING activation.
(A) Schematic of RUSH-STING system. **(B)** Confocal microscopy of Hela Kyoto cells expressing RUSH-STING under indicated conditions. DAPI in blue, STING (FLAG) in green and TGN46 in magenta. **(C)** Quantification of STING-Golgi colocalization from images in (B). Colocalization was done through FIJI and Python script computing the percentage of STING pixels overlapped with Golgi pixels relative to total STING pixels. **(D)** Western blot showing activation of the STING pathway in HEK293T cells expressing pcDNA-STING-FLAG (left) and RUSH-STING-FLAG (right). Biotin treatment allows the release of the RUSH construct from the ER-localized hook and enables any natural trafficking process to occur. Quantitation of blots is provided in Figure S2. **(E)** IFN-β stimulation as measured by a luciferase reporter of pcDNA-STING-FLAG (left) and RUSH-STING-FLAG (right) expressed in 293T-Dual cells.

Figure 3. Palmitoylation at C64 alone but not C91 is necessary for activation and prevents non-productive oligomers.

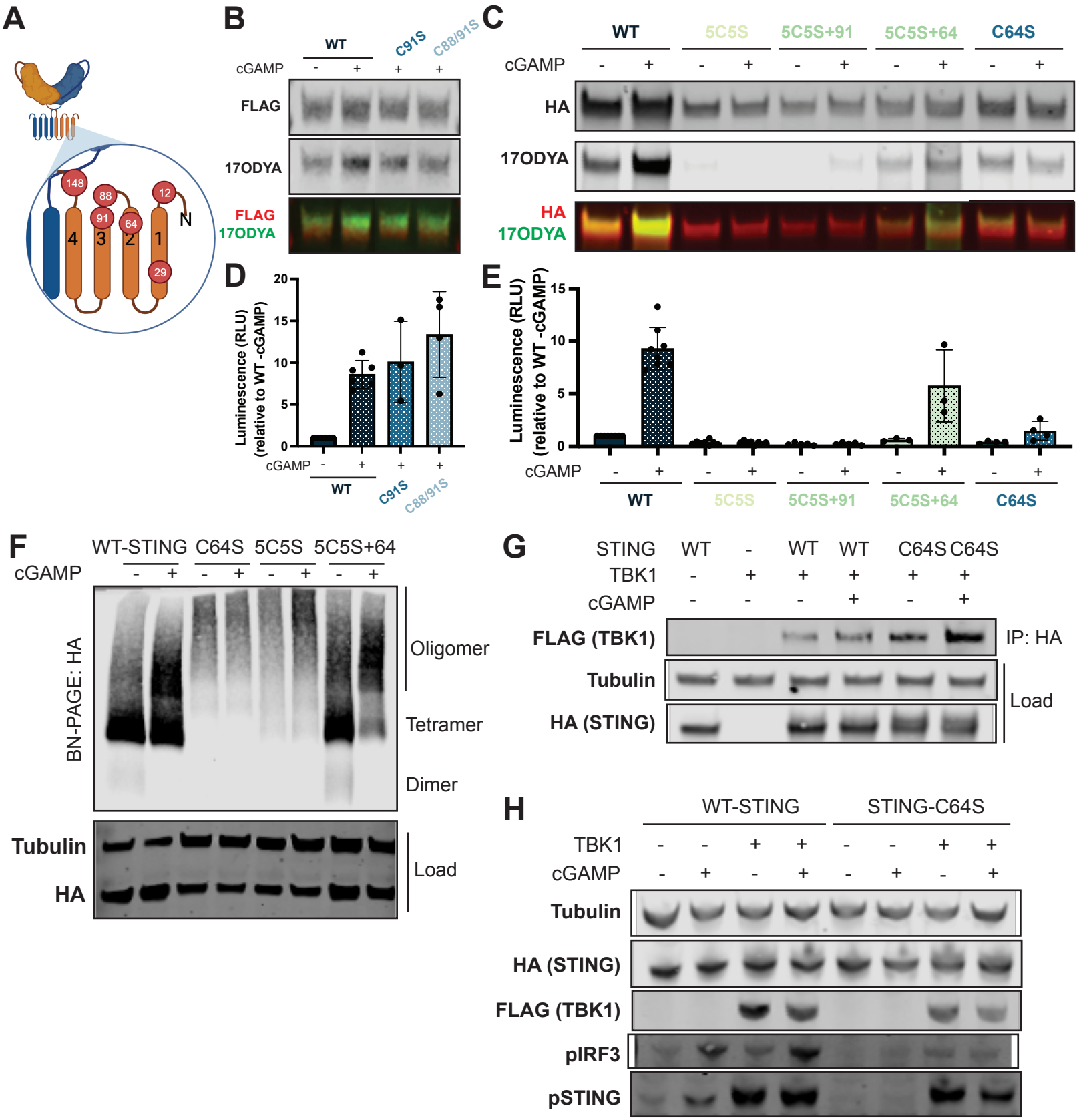

Figure 3. Palmitoylation at C64 alone but not C91 is necessary for activation and prevents non-productive oligomers.

(A) A cartoon depicting the relative positions of the five transmembrane cysteine residues. **(B, C)** 17-ODYA palmitoylation assay from HEK293T cells expressing STING variants. **(D, E)** Relative IFN-β secretion from HEK293T-Dual reporter cells expressing STING variants. **(F)** Blue-native PAGE of Hela Kyoto cells expressing indicated STING variants. **(G)** Co-immunoprecipitation of TBK1-FLAG with either WT-STING-HA or STING-C64S-HA from HEK293T cells. **(H)** Phospho-IRF3 and phosphor-STING levels of HEK293Ts co-expressing TBK1-FLAG and either WT-STING-HA or STING-C64S-HA.

Figure 4. C91-reactive compounds allosterically alter C148 reactivity and dimerization.

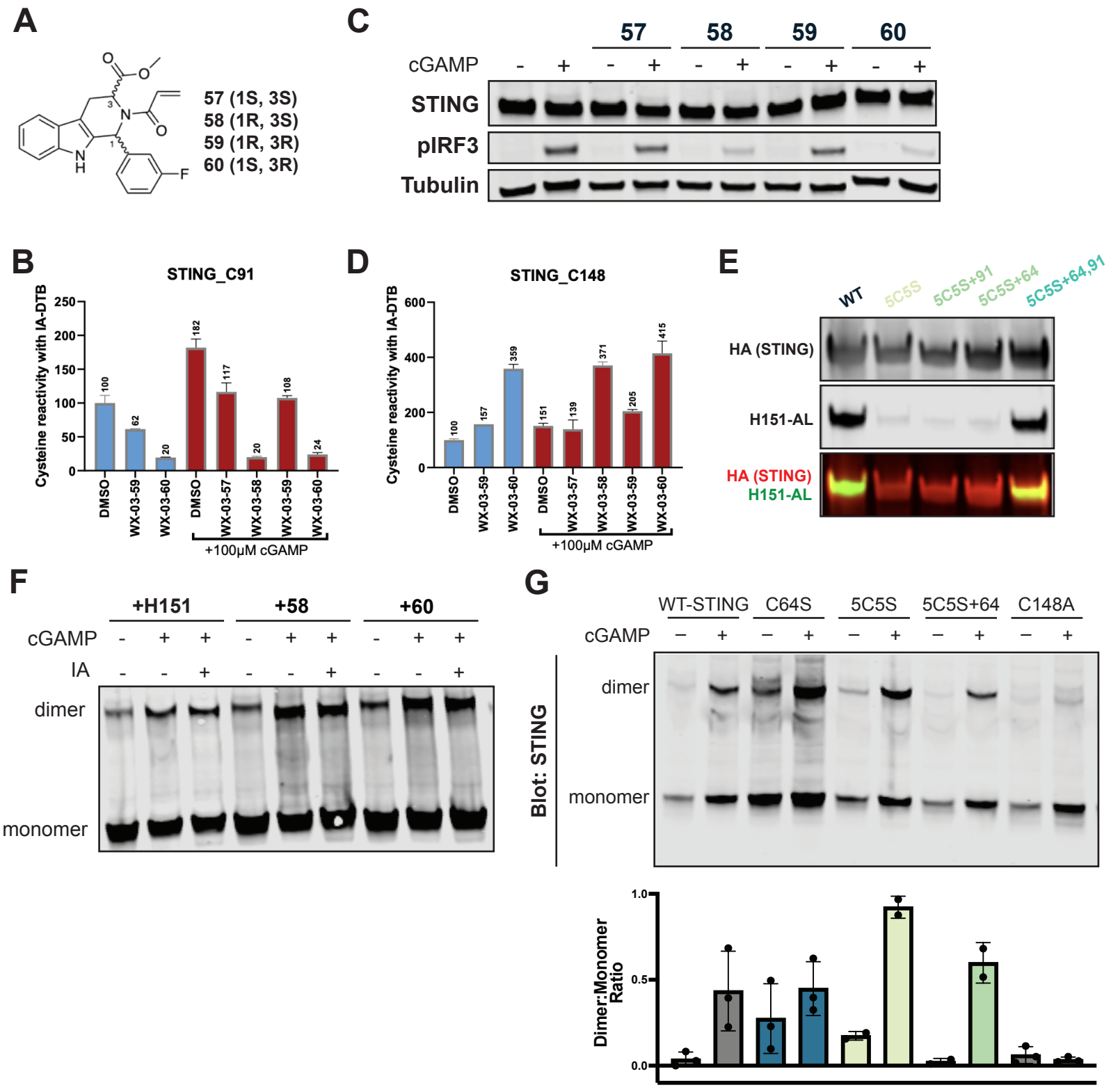

Figure 4. C91-reactive compounds allosterically alter C148 reactivity and dimerization.

(A) Structure of four cysteine-reactive stereoisomers, where two stereoisomers (**58** and **60**) inhibited STING signaling. **(B)** Changes in C91 reactivity relative to DMSO control upon different compound and cGAMP treatment conditions in THP-1 cells. Cells were either treated with compound alone or both compound and cGAMP concurrently. **(C)** Compounds **57** to **60** were assessed in U937 for their ability to inhibit cGAMP-induced STING signaling. **(D)** Changes in C148 reactivity relative to DMSO control upon different compound and cGAMP treatment conditions in THP-1 cells. **(E)** H151-AL incorporation assay with STING variants in HEK293T cells. **(F)** Non-reducing SDS PAGE of HEK293T cells expressing WT-STING and pre-treated with C91-reactive compounds. **(G)** Non-reducing SDS-PAGE of HEK293T cells expressing STING variants, with or without treatment by cGAMP. Quantification is represented below as the ratio of intensity of dimer to monomer bands. For (C), (F) and (G), cells were pre-treated with the indicated compound at 5 μM for 2 hours before a further 2-hour treatment with 100 μM cGAMP.

Figure 5. A C-terminal tail-derived fragment targets a location on STING to inhibit oligomerization and activation

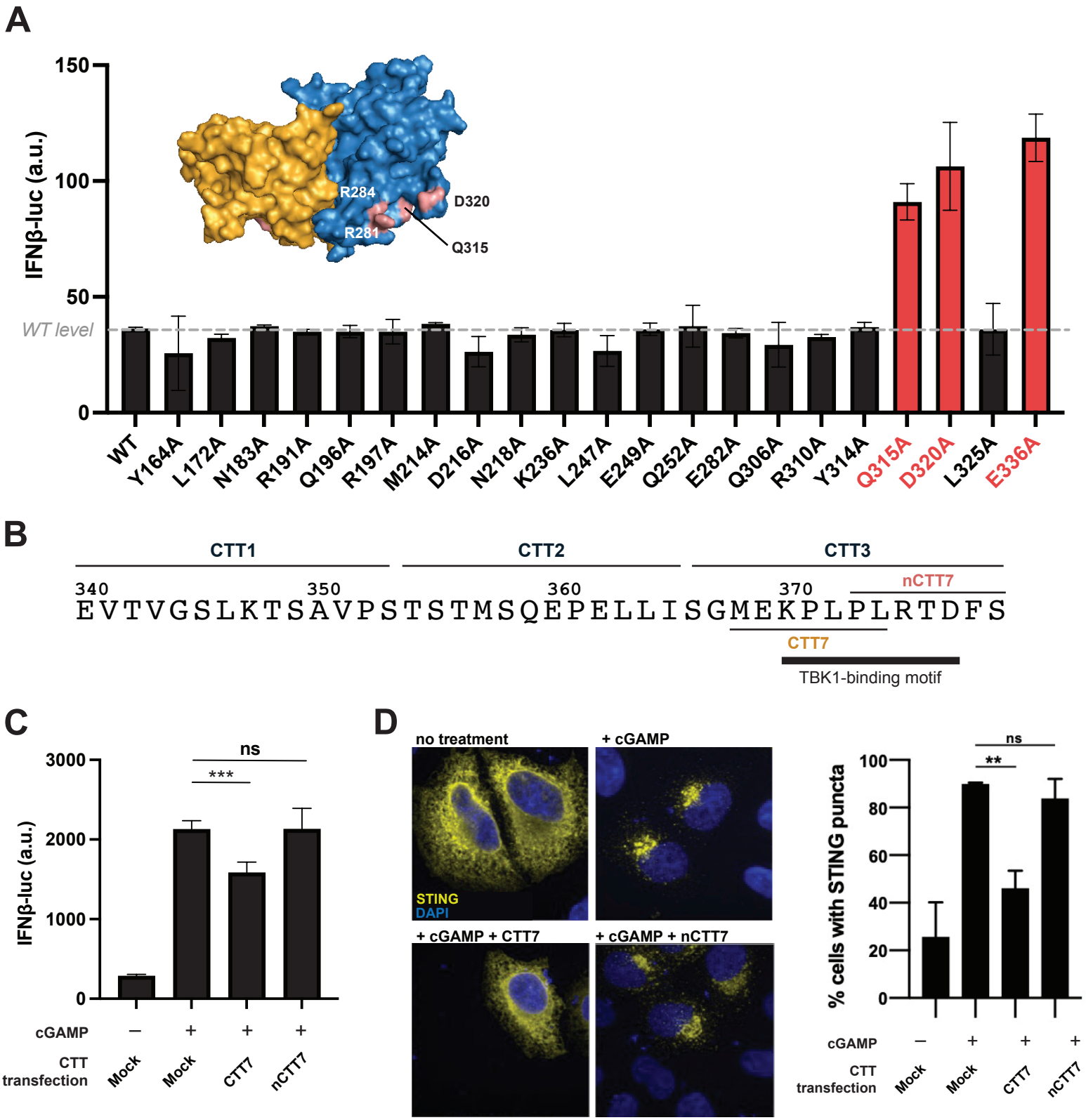

Figure 5. A C-terminal tail-derived fragment targets a location on STING to inhibit oligomerization and activation.

(A) Relative IFN-β secretion from HEK293T-Dual reporter cells expressing a panel of alanine mutants of residues on the STING surface. Constitutively active mutants that suggest loss of STING autoinhibition are shown in red. **(B)** Residue sequence of STING's C-terminal tail. Three truncated units (CTT1–3, labelled) were first evaluated for STING affinity (Figure S5). The binding and inhibitory fragment CTT3 was then further truncated into a minimal peptide capable of inhibiting STING signaling (CTT7) and control peptide (nCTT7). **(C)** Relative IFN-β secretion from HEK293T-Dual reporter cells co-expressing WT STING and CTT7-FLAG constructs. **(D)** Confocal microscopy of Hela Kyoto cells co-expressing WT-STING and CTT7-FLAG constructs. Corresponding quantification of percentage of cells with STING puncta also shown.

Figure 6. CTT is an inhibitor of STING–STING interaction

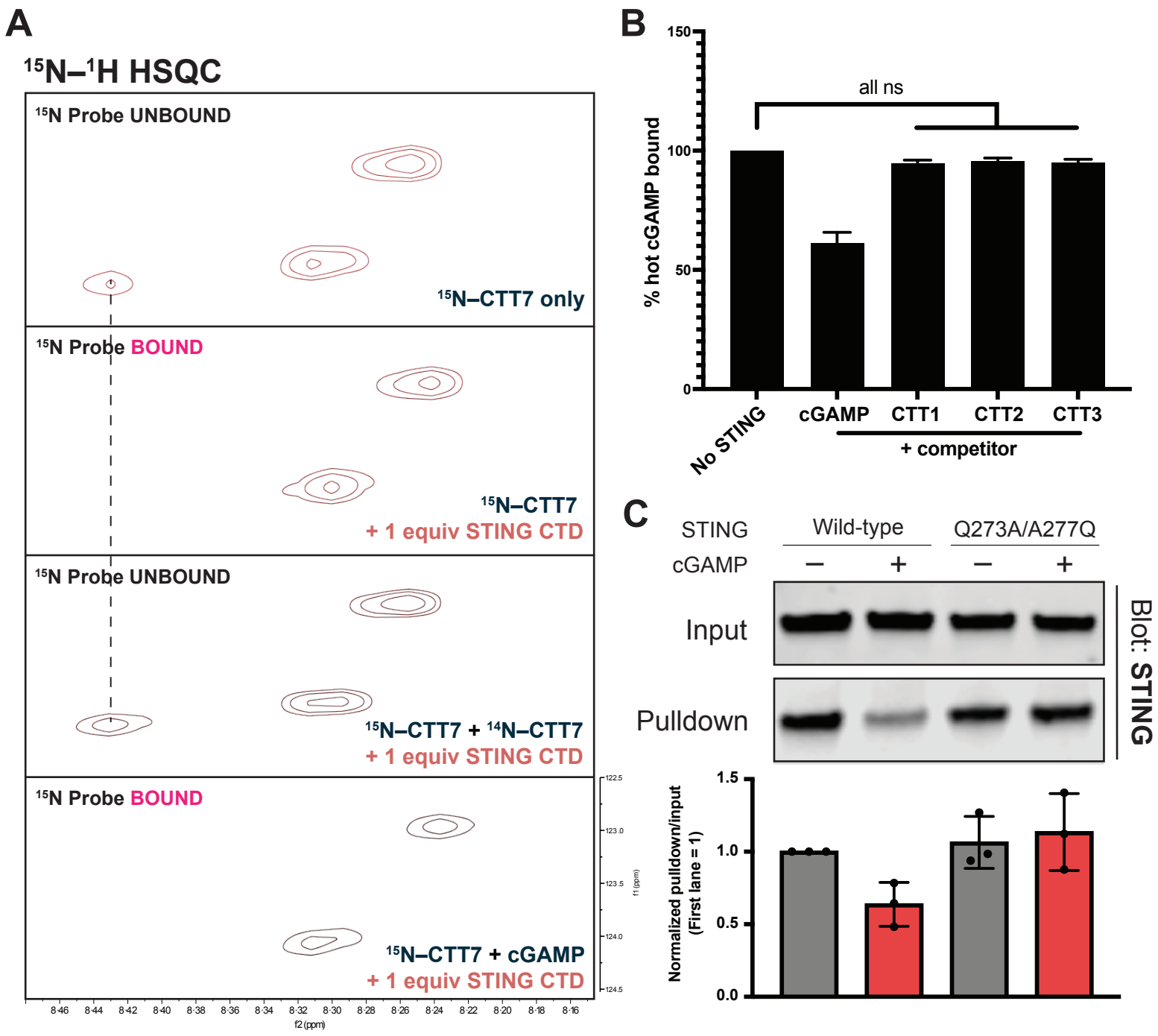

Figure 6. CTT is an inhibitor of STING-STING interaction.
(A) Comparison between the 15N-1H HSQC spectra obtained for 1.5 mM ^{15}N-CTT7 alone (panel 1), with one equivalent of STING CTD (panel 2), with one equivalent of both STING CTD and non-isotopically labelled CTT7 (panel 3), and one equivalent each of STING CTD and cGAMP (panel 4). **(B)** Radioactivity assay of ^{32}P-labelled cGAMP bound to purified STING CTD in the presence of cold cGAMP or various fragments of STING's CTT (CTT1, CTT2, CTT3). **(C)** Co-immunoprecipitation assay of CTT7 peptide with either WT-STING or STING-Q273A/A277Q, an oligomerization defective mutant. Corresponding quantification of pulldown normalized to input also shown.

Figure 7. CTT7 binds at a site exhibiting residue-activity relationship

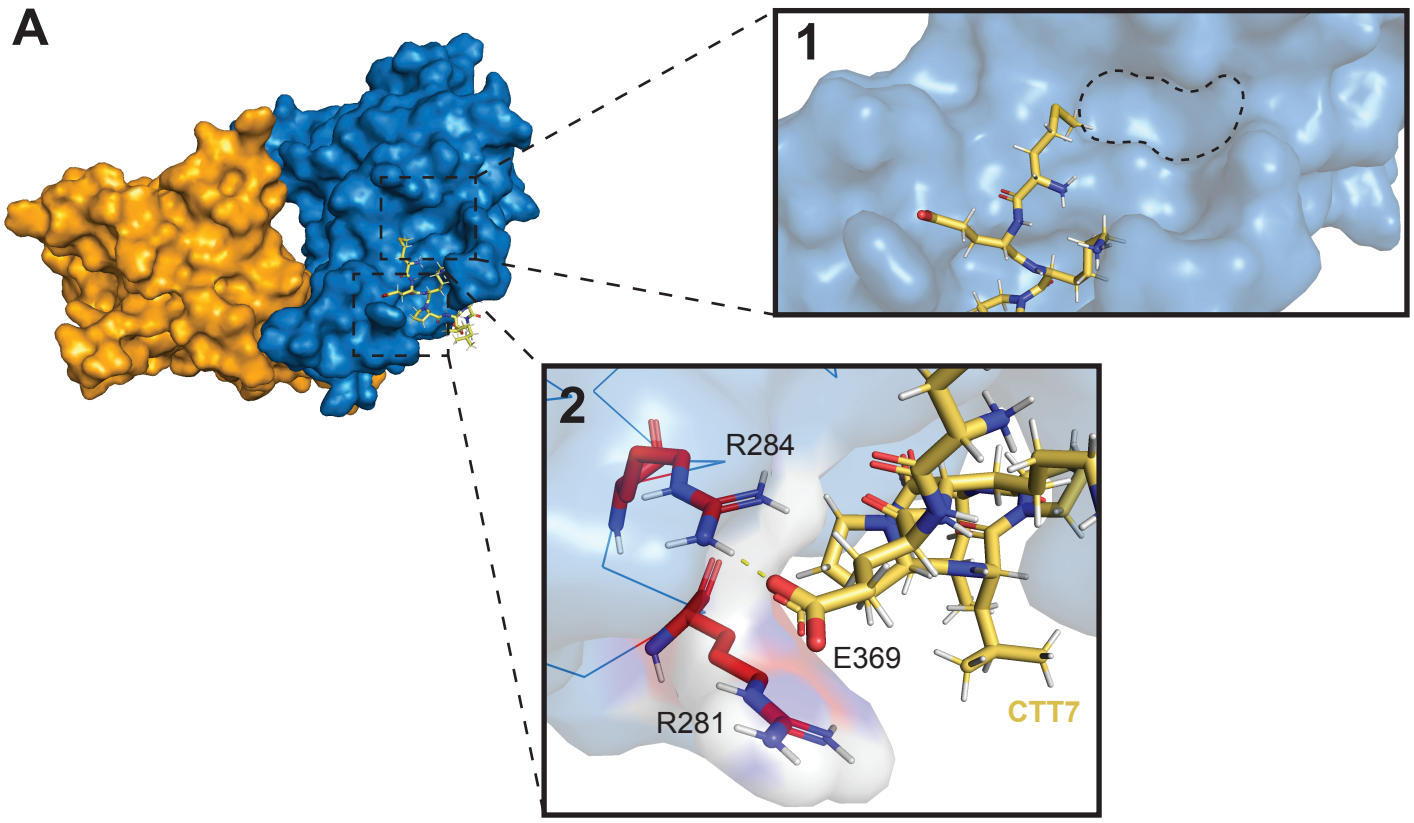

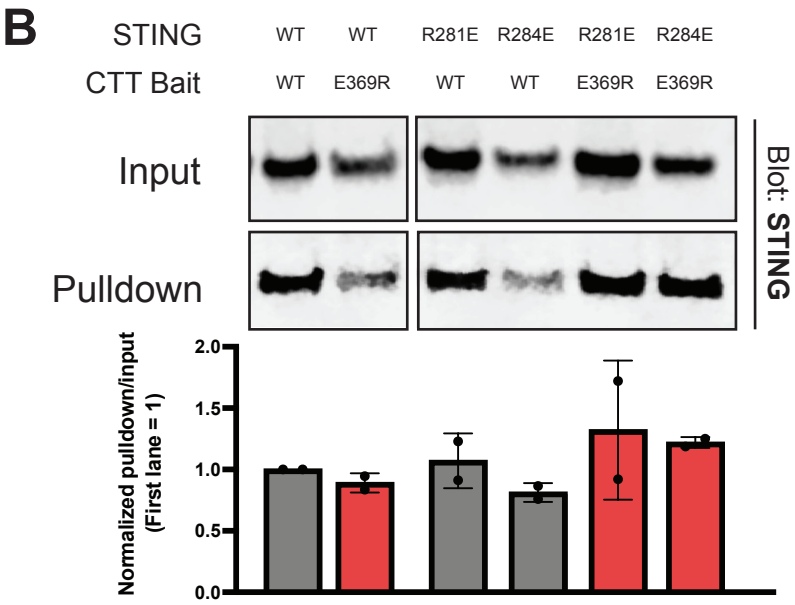

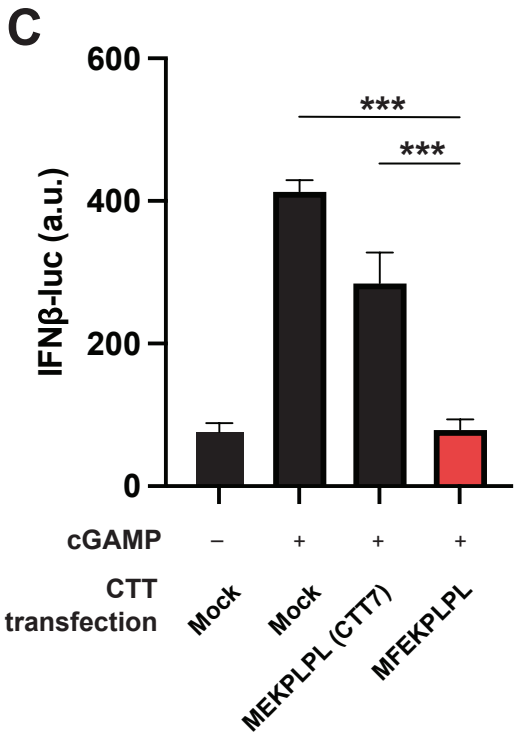

Figure 7. CTT7 binds at a site exhibiting residue-activity relationship.
(A) Molecular docking of CTT7 onto STING CTD. Inset 1 reveals an unoccupied hydrophobic pocket-like site. Inset 2 shows a candidate binding site for CTT7 on STING, with potential interacting residues shown. **(B)** Co-immunoprecipitation assay using either WT-CTT7 (gray bars in quantification) or CTT7-E369R (red bars) as bait and pulling down WT STING or charge mutants. Quantification shown below of pulldown normalized to input. **(C)** Relative IFN-β secretion from HEK293T-Dual reporter cells co-expressing WT-STING with either CTT7 or a lengthened CTT fragment that more potently suppresses STING signaling.

Figure 8. Revised model for STING activation

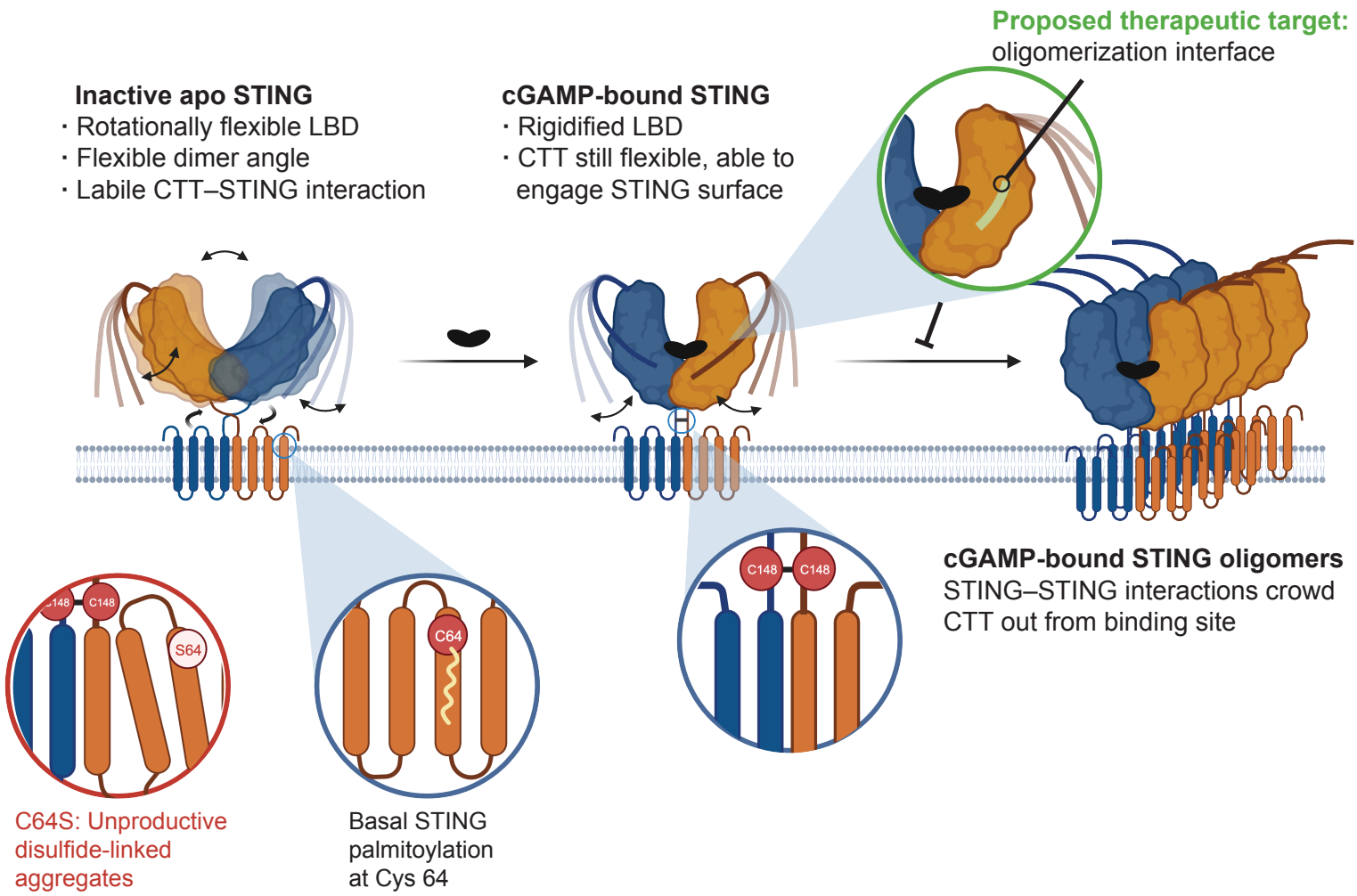

Figure 8. Revised model for STING activation.

When inactive, STING's cytosolic domain remains flexible rotationally and within the dimer angle with dynamic CTT interactions. Within the transmembrane domain, STING is also basally palmitoylated which is key to STING forming productive oligomers rather than unproductive aggregates. Upon cGAMP binding, the STING body is rigidified, with the CTT remaining flexible and able to engage the STING surface. This rigidification promotes the formation of productive C148 intradimer disulfide linkages that further stabilize STING. This more fixed, cGAMP-bound STING is then better able to interact with neighboring STING dimers at the oligomerization interface, outcompeting STING's own CTT from binding this site and making them more available for downstream effector binding.

Supplementary Figure 1

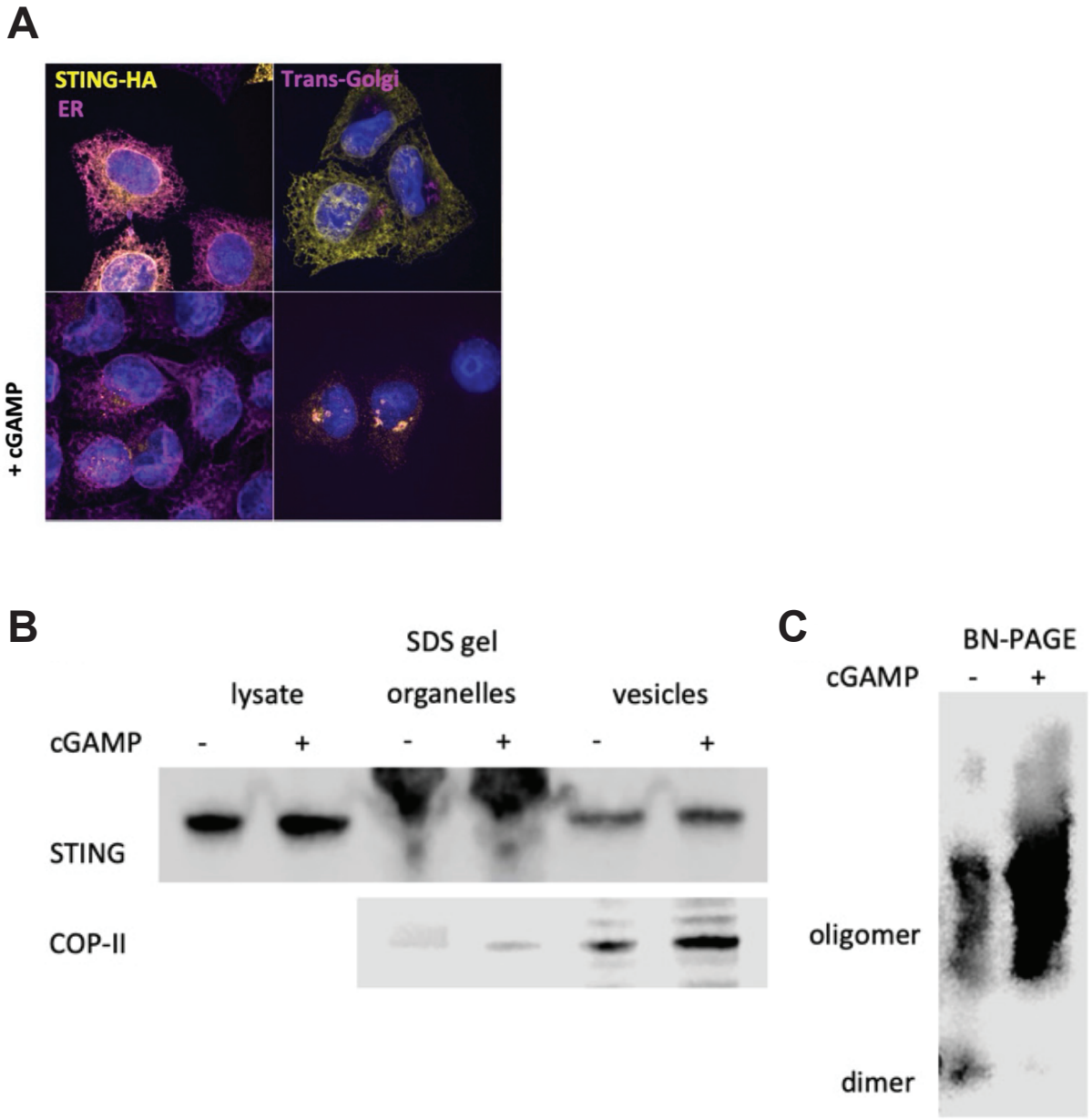

Supplementary Figure 1, related to Figure 1.

(A) Confocal microscopy of Hela Kyoto cells expressing WT-STING-HA, showing localization with and without cGAMP. **(B)** SDS-PAGE gel of vesicles enriched through cellular fractionation, as demonstrated by enhancement of COP-II proteins. **(C)** Blue-native PAGE of vesicle-enriched fraction from (B).

Supplementary Figure 2

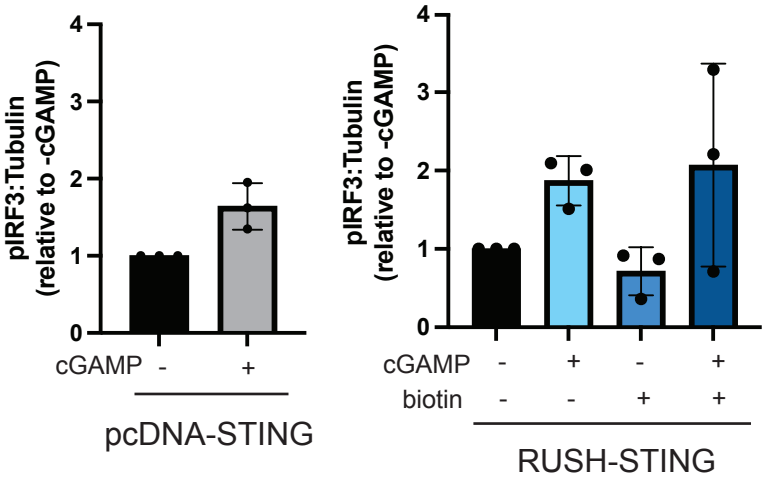

Supplementary Figure 2: related to Figure 2.

Quantitation of data from Figure 2 as normalized intensity of pIRF3, over three independent experiments.

Supplementary Figure 3

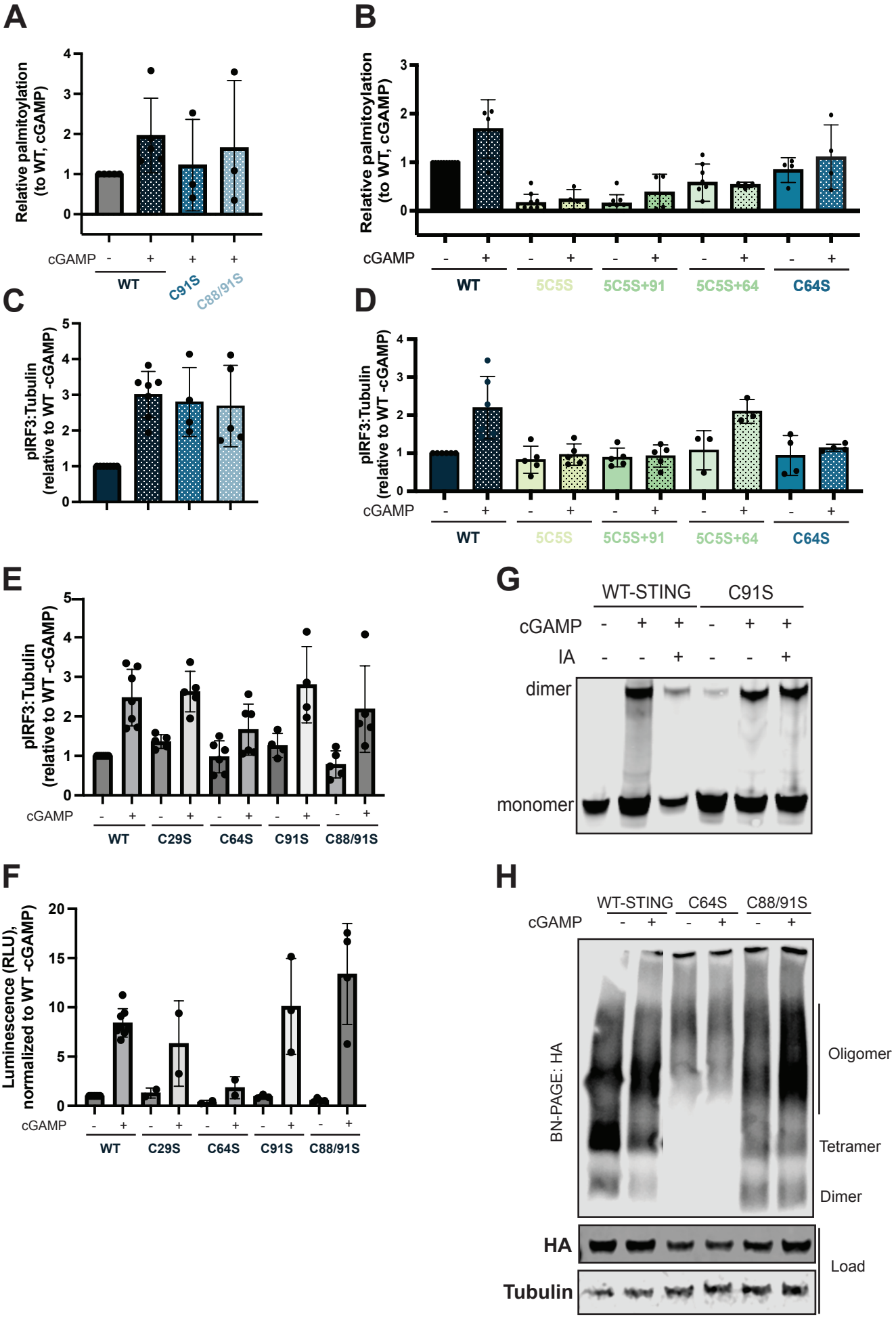

Supplementary Figure 3: related to Figure 3.

(A, B) Quantification of Western blots shown in Figures 3B (A) and 3D (B). Data shown is from three independent experiments with error bars representing standard error of mean. **(C, D)** Relative pIRF3 of HEK293Ts in the same condition as in Figures 3B and 3D. **(E)** Relative pIRF3 of HEK293Ts expressing cysteine mutants of four cysteines within the transmembrane domain. **(F)** Relative IFN-β secretion from HEK293T-Dual reporter cells expressing the same mutants. **(G)** Non-reducing SDS-PAGE of WT-STING and STING-C91S. **(H)** Blue-native PAGE of WT-STING, STING-C64S, and STING-C88/91S, showing preventing palmitoylation at C88/91 does not induce aggregate formation.

Supplementary Figure 4

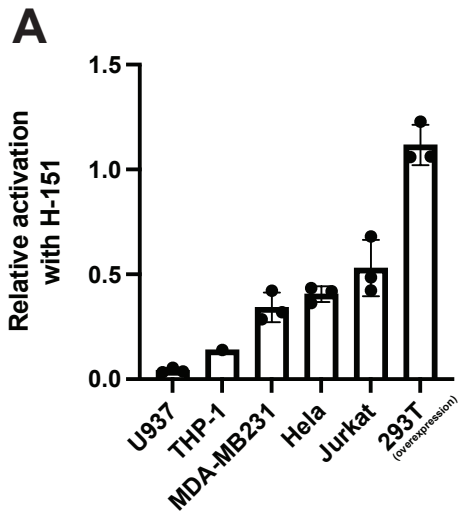

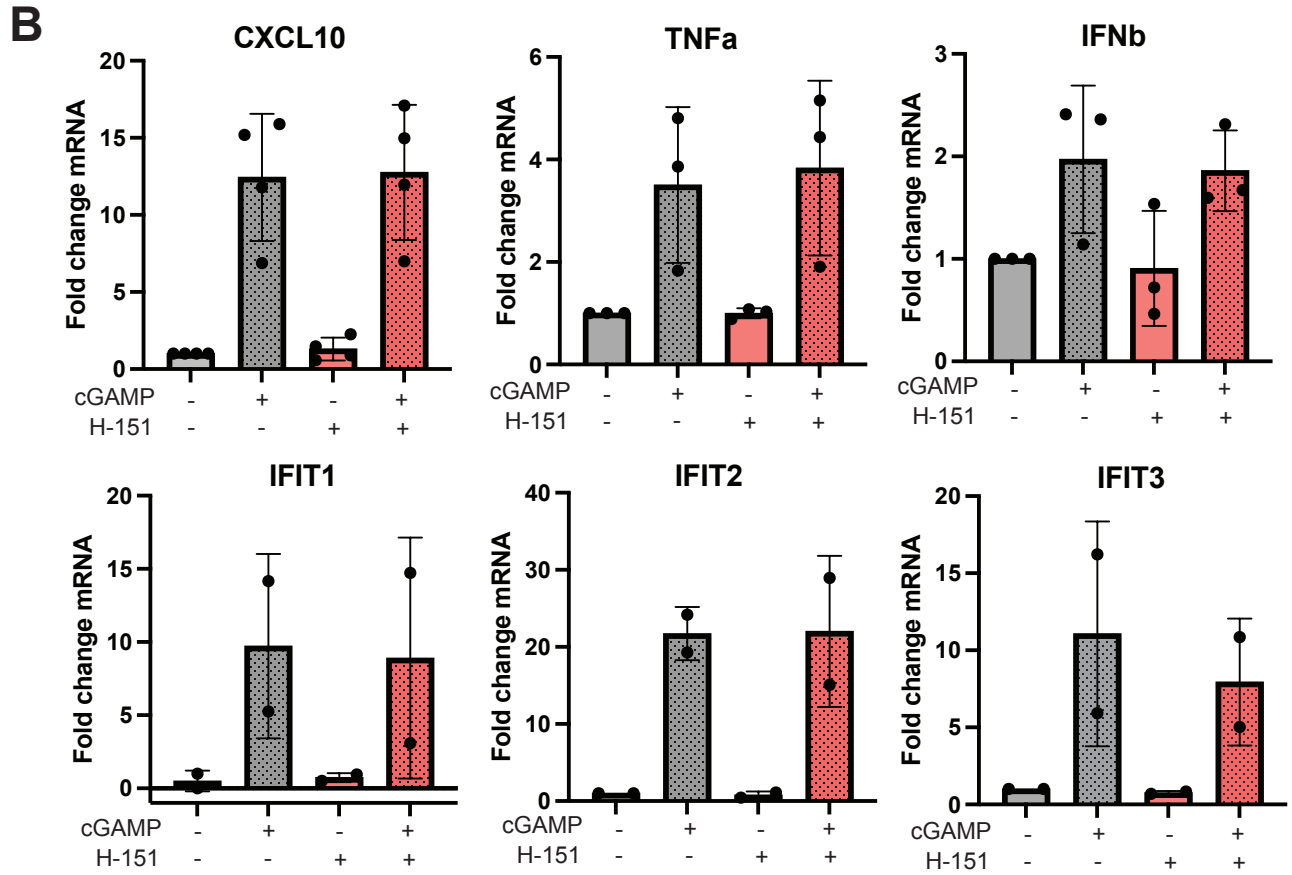

Supplementary Figure 4: related to Figure 4.

(A) Relative pIRF3 levels of H-151 treated cells stimulated with cGAMP, compared to cGAMP stimulation alone, amongst a panel of cell lines. **(B)** RT-qPCR of downstream cytokine mRNA levels in peripheral blood mononuclear cells (PBMCs) under indicated conditions.

Supplementary Figure 5

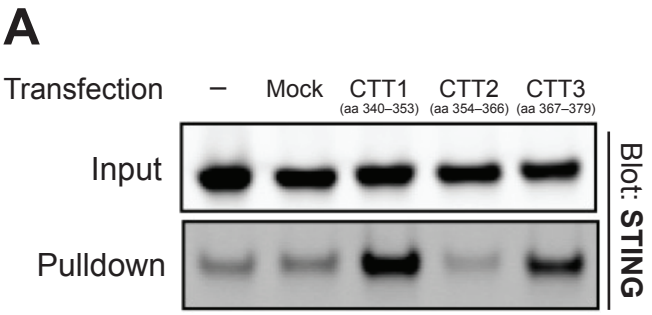

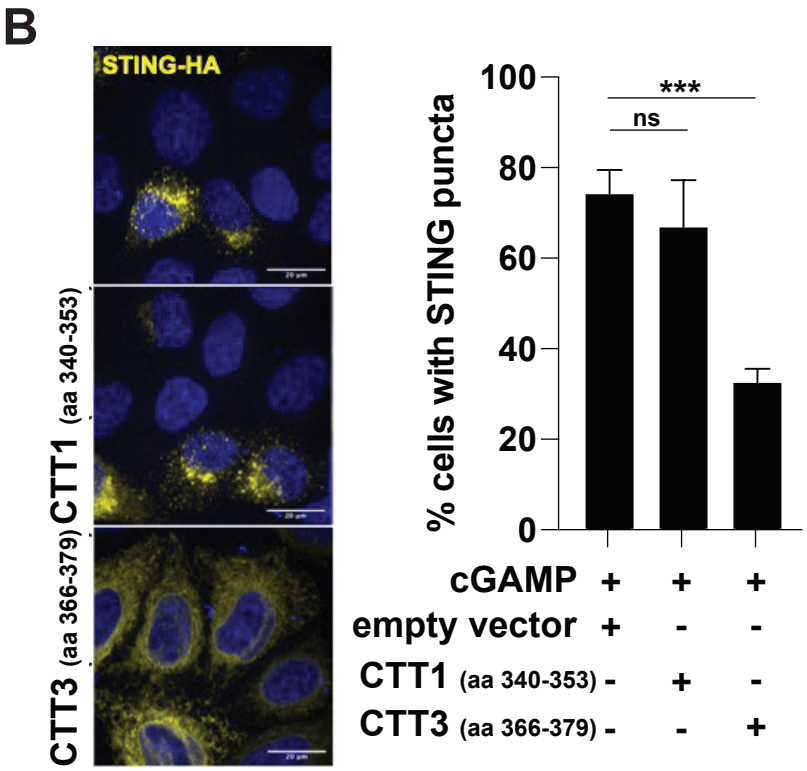

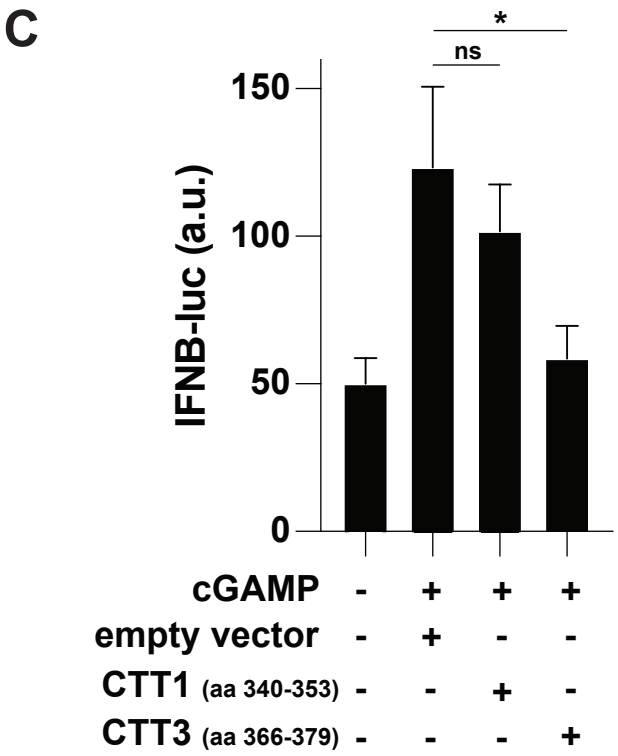

Supplementary Figure 5: related to Figure 5.

(A) Co-precipitation assay of HEK293T cells transfected with WT-STING and various CTT truncations to determine which region of the CTT interacts with STING. **(B)** Confocal microscopy of Hela Kyoto cells co-expressing WT-STING-HA with CTT truncations. Quantification shows the percentage of cells with STING puncta in these conditions.

Supplementary Figure 6

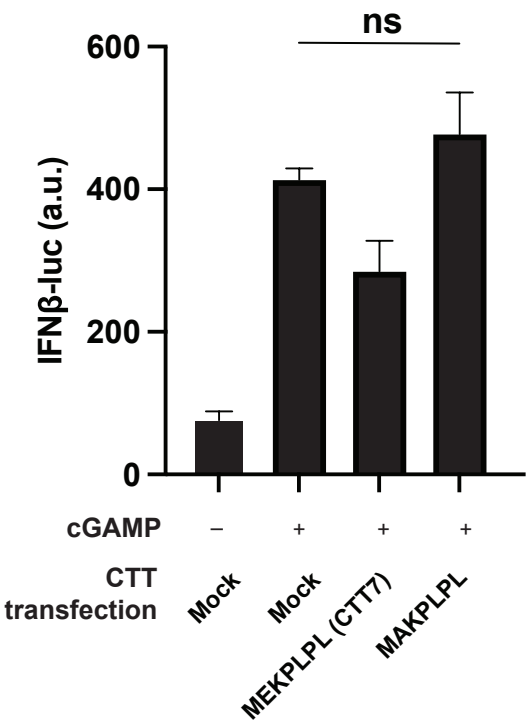

Supplementary Figure 6: related to Figure 7.
Relative IFN-β secretion from HEK293T-Dual reporter cells co-expressing WT-STING with CTT7 and a version of CTT7 that does not inhibit signaling, E369A-CTT7.